ASPECTS OF A SPHERICALLY SYMMETRIC MODEL OF THE POST-DECOUPLING UNIVERSE

A dissertation submitted
to

The Department of
MATHEMATICS and APPLIED MATHEMATICS
at
the University of Cape Town

in fulfillment of the requirements for the degree
of

MASTER OF SCIENCE

in

APPLIED MATHEMATICS

By
Nazeem Mustapha
September 1996

Contents

1 Introduction **1**
1.1 Aims . . . 3

2 The Lemaître-Tolman-Bondi Model **6**
2.1 Close Relatives . . . 6
2.2 Description . . . 9
2.2.1 The Friedmann-Lemaître-Robertson-Walker limit . . . 13
2.2.2 Behaviour at the Origin . . . 14
2.3 Singularities . . . 16
2.3.1 Shell Crossings . . . 18
2.3.2 The Shell Focussing Singularity . . . 21

3 Effect of Radial Lensing on Distance Measurements **23**
3.1 Gravitational Lensing . . . 23
3.1.1 Strong and Weak Lensing . . . 24
3.2 Shrinking and Magnification Caused by Radial Lensing . . . 28
3.2.1 Programme . . . 30
3.2.2 Results . . . 37
3.2.3 Conclusions . . . 49

4 Clumps Evolving to Voids **51**
4.1 Preliminaries and Programme . . . 54
4.1.1 Procedure . . . 55
4.1.2 The Hyperbolic Case . . . 57
4.2 Density Profile Inversion: Existence Proof . . . 68
4.3 Specific Models . . . 71
4.4 Implications and Discussion . . . 79

5 Conclusion **81**

List of Abbreviations

CDM	Cold Dark Matter
CH	Copernican Hypothesis
CMB	Cosmic Microwave Background
DPI	Density Profile Inversion
EFE	Einstein Field Equations
FL	Friedmann-Lemaître
FLRW	Friedmann-Lemaître-Robertson-Walker
GR	General Relativity
HDM	Hot Dark Matter
LTB	Lemaître-Tolman-Bondi
LRS	Locally Rotationally Symmetric
RW	Robertson-Walker

List of Figures

3.1 (Adapted from [61].) The wavefronts in a typical lensing system. Close to the source the wavefronts (dashed lines) are nearly spherical, but as they approach the deflector, they become deformed and may self-intersect forming caustics. Every passage of the wavefront past the observer corresponds to an image of the source in the direction of the light rays (solid lines), perpendicular to the wavefront. This illustrates the well known theorem that an odd number of images of a source are detected for a multisheeted wavefront. For radial lensing there is no bending of the wavefront at all; only a uniform early or late arrival of the wavefronts, when compared with a smooth model, occurs. . . . 25

3.2 A plot of area distance against redshift on the past null cone of the inhomogeneous model LTB1 and the corresponding FL background area. The units of $\hat{R}$ are cosmological length units, and all the figures use base 10 logs. This shows that there are systematic shrinking ($\hat{R} > \hat{R}_{FL}$) and magnification ($\hat{R} < \hat{R}_{FL}$) effects due to purely radial lensing, which obviously cannot be removed by averaging over large angular scales or even the whole sky. Effects of true lensing in a more realistic universe would be imposed on top of this. 42

3.3 The density of matter on the *past null cone* (that is, what would actually be observed) in the models of Figure 3.2, LTB1 and its corresponding background FL model. The units are cosmological density units ($cmu\ clu^{-3}$). When comparing with Figure 3.2, we see that roughly speaking, magnification occurs for objects in or just beyond an overdense region, and shrinking occurs for objects in or just beyond an underdensity. 43

3.4 The LTB area distance function $\hat{R}(r)$ on the past null cone and its background FL analogue ($\hat{R}_{FL}$) for the second LTB model, LTB2, given in cosmological units. The horizontal variable is $v = r/t_u$ or r/t_b for LTB2 and FL respectively. The physical behaviour of LTB2 as plotted against v appears normal. 45

3.5 The densities for the second LTB model and its background FL model ($\hat{\rho}$ and $\hat{\rho}_{FL}$, in cosmological units) on the past null cone. Again, LTB2's inhomogeneous profile vs v appears quite acceptable. 46

3.6 A plot of area distance against redshift for model LTB2 and the background FL model. The interesting point to note is that at some redshifts the area distance in the LTB model is multivalued. For $\log_{10}(1+z) \geq 1$ the graph looks very much like Figure 3.2. 47

3.7 The densities ($\hat{\rho}$ and $\hat{\rho}_{FL}$) on the past null cones vs z for model LTB2 and its background FL model. Note the quaint 'looping' behaviour. For $\log_{10}(1+z) \geq 1$ the graph looks very much like Figure 3.3. 48

4.1 A projection onto the plane of a 3000 km/s thick slice of Tony Fairall's compilation of all published redshifts for galaxies in the Southern hemisphere added to the redshifts from ZCAT compiled by John Huchra for the Northern hemisphere. No selection criteria have been taken into account. The axes are in km/s. The apparent radial alignment some of these galaxies exhibit are the well known 'fingers of God' effect. They are due to the fact that galaxies within bound clusters exhibit a large range of peculiar motions which is not taken into account by surveyors, as it is assumed all shifts are due to motions directly from or towards us. (Courtesy Paul Haines.) 52

4.2 The η-functions complementary to the first three terms in $(R')^4 \times (\partial_{RR}\rho) \,/\, \rho$. The function labelled as f_2 rises to a maximum of just below -22.55 before asymptotically tending to -23. 65

4.3 The η-functions in $(R')^4 \times (\partial_{RR}\rho) \,/\, \rho$ complementary to the fourth to sixth terms. 66

4.4 The η-functions in $(R')^4 \times (\partial_{RR}\rho) \,/\, \rho$ complementary to the seventh to ninth terms. The function f_7 asymptotically tends to 1. 66

4.5 The η-functions in $(R')^4 \times (\partial_{RR}\rho) \,/\, \rho$ complementary to the tenth to thirteenth terms. 67

4.6 The density profile on a worldline at an early time ($t = 1 \times 10^{-6} \sim 2000yrs$). In these figures, the core is taken to be the value of R at the comoving radius $r = 0.04$ and they all use base 10 logs. At this time the value corresponds to an overdensity of about 1.7 kpc in diameter which corresponds to the size of a small galaxy today. The units in all the figures are cosmological. The value of the density at the origin $\rho_0 \sim 2.0 \times 10^{-16} g/cc$. 75

4.7 The density profile on a worldline at a later time. This diagram and the next one illustrate the change in concavity at the centre, which occurs when the universe was $\sim 2 \times 10^4$ years old. $R \sim 7.9kpc$ and $\rho_0 \sim 2.0 \times 10^{-18} g/cc$. . . . 76

4.8 The density profile on a worldline at a still later time which, when compared to the previous figure, illustrates the movement of the maximum away from the centre. This is as we expected and shows that a density wave must exist near the origin if the profile inverts on the central worldline. $t \sim 4 \times 10^4 yrs$, $R \sim 12.5kpc$ and $\rho_0 \sim 5 \times 10^{-19} g/cc$. 77

4.9 The density profile on the worldline today ($t \sim 20Gyrs$). This corresponds to a void (albeit one with a rather elongated wall) with a diameter of approximately $100Mpc$. $\rho_0 \sim 5 \times 10^{-31} g/cc$ and the maximum density on this diagram is $\rho_m \sim 10^{-3.5} \sim 1.2 \times 10^{-30} g/cc$. 78

List of Tables

2.1 The Conditions for No Shell Crossings. 19

3.1 Correspondence Between Cosmological, SI and Astronomical Units 38

4.1 Restrictions imposed on the perturbation t_B by the requirement of a flat central density ($\forall c \in \mathbb{N}^+$) 72

4.2 Restrictions imposed on the perturbations to E and M by the requirement of a flat central density ($\forall a, b \in \mathbb{N}^+$) 73

4.3 The late time value of $(\partial_{RR}\rho)/\rho$ at the origin multiplied by M_0. 74

I celebrate myself, and sing myself,
And what I assume you shall assume,
For every atom belonging to me as good belongs to you.

– Walt Whitman

Chapter 1

Introduction

At first it will be difficult.

But then all things are difficult ... at first.

– Myamoto Mushashi

Modern Cosmology uses the Einstein Field Equations (EFE)

$$G_{ab} = R_{ab} - \frac{1}{2}g_{ab}R + \Lambda g_{ab} = 8\pi G T_{ab} \tag{1.1}$$

in an attempt to understand and describe the universe on large scales, with constraints provided by observations and by deductions based on other branches of physics. The Einstein tensor G_{ab} is defined in terms of the Ricci tensor R_{ab} and Ricci scalar R and may be derived from the metric tensor g_{ab} thus representing the space-time geometry. T_{ab}, the energy momentum tensor, describes the substance that fills the universe which, for the post-decoupling[1] era, is usually taken to be matter and radiation in a fluid state. Λ is the cosmological constant and G is Newtons gravitational constant.

On large enough scales at recent times it generally is assumed that the dynamics of the universe can be described by massive particles (galaxies) whose interactions are purely

[1] Decoupling here refers specifically to the decoupling of photons from the baryons (that is the matter becoming transparent) which occurred at an epoch when the cosmic temperature dropped below the ionisation temperature of hydrogen. Thus this is also often referred to as recombination. After decoupling, the photons do not scatter off the electrons anymore and start free-streaming and thus the surface on which this occurs is called the surface of last scattering.

gravitational: that is, they follow geodesics on a curved space-time. Although gravity is the weakest of the known forces, neither gas pressure, nor electromagnetic, nor any other force is significant on such cosmological scales; so this is a reasonable assumption as long as the particles are sufficiently large. By contrast, within galaxies, neutral and ionised cosmic gas (e.g. HI and HII regions) constitutes a large fraction of their masses, and the dynamics of ionised gas is strongly influenced by pressure and magnetic fields. The electro-magnetic force is a long range force stronger than gravity, but since gravity does not allow positive and negative charges, it dominates on large scales. Because the number of galaxies and clusters in the observed universe is extremely large with small relative velocities, the matter in most of the universe is probably well described by a pressureless fluid. This approximation is not valid prior to recombination – when pressure is large. It would be cast into doubt if it turns out that there is a significant amount of hot dark matter (HDM) with a strange equation of state.

The Friedmann-Lemaître-Robertson-Walker[2] (FLRW) model, which is isotropic and homogeneous with a perfect fluid energy-momentum tensor, is the standard one used by most astronomers, astrophysicists and cosmologists. Despite the success this model enjoys in describing the observed universe, it lacks the requisite richness that has been seen on all scales. With the discovery of large scale inhomogeneities it has become increasingly important to study deviations from this model. One way to do this is to study perturbations of the standard model. This is a major field of study fraught with many conceptual and technical difficulties. But there are exact solutions of the EFE which are often adequate for investigating important features absent from the standard model. Some of these features are the subject of this thesis.

[2]We follow recent moves to use 'Friedmann-Lemaître' (FL) to describe the dynamics of and the application of the Einstein field equations to the standard model, and 'Robertson-Walker' (RW) to describe its metric and geometry.

1.1 Aims

The central aim of this thesis is to consider aspects of the spherically symmetric Lemaître-Tolman-Bondi (LTB) solution as a model of the post-decoupling universe. To do this comprehensively is a massive task and is not our aim here. Indeed, far from it, we will concentrate on select instances of this programme and attempt in some places to indicate possibilities for further study.

There are many solutions of the EFE which satisfy what we consider to be 'reasonable criteria' for a cosmology and others that do not. The LTB solution may be accepted as a reasonable cosmological model because

- It allows non-empty solutions.
- It allows expanding solutions.
- It has a homogeneous and isotropic limit.
- It allows for inhomogeneity.

The first of these is quite obviously necessary and the second has been well established for over sixty years. We regard the fourth one as a non-trivial assumption, because for many years the FLRW geometry was – and still is, to a large extent – regarded by workers in the field as *the* model of the universe. However the observations of large inhomogeneities in the late 70's and 80's[3] and, for instance, the mathematical study by Tavakol and Ellis (1988) [67] which implied that the set of FLRW models is probably structurally unstable, suggests the inclusion of the fourth as a possibly crucial assumption. We acknowledge the need for the third criterion, because observations of the Cosmic Microwave Background Radiation (CMB) have, fairly conclusively, shown that at a very large scale (probably much greater than

[3]which is still in progress: The Sloan Digital Sky Survey is expected to obtain a three-dimensional map out to $z \approx 1$ with more than a million galaxy redshifts.

1000 Mpc) the universe is nearly isotropic[4]. The results at the time of writing are that the temperature of the CMB deviates from isotropy at the level $(\Delta T/T)_{rms} \approx 1.1 \times 10^{-5}$ on angular scales $\geq 10°$ once the dipole is removed. The Copernican Hypothesis (CH), which simply put says that there are no preferred worldlines, is implicitly added to these criteria by most cosmologists. It, together with the near-isotropy of the CMB, implies that the universe is nearly-FLRW [65] (hence the need for a homogeneous and isotropic FLRW limit). CH is not satisfied in the general LTB model, because the spherical symmetry means that there *is* a preferred centre of coordinates. On the other hand, the Robertson-Walker models satisfy CH, but they do not allow for any meaningful structure. Yet, it must be remembered that CH is a philosophical assumption – indeed, a working hypothesis – and, whilst plausible, it cannot be tested observationally [19] at present[5]. Although galaxy counts against redshift or magnitude are consistent with a homogeneous universe in the redshift range $0.03 \leq z < 0.3$, by $z \approx 4$ this does not hold true any longer for counts to the blue side unless we assume evolution of sources[6]. Thus the geometry of the universe can certainly not be detected from observations of galaxies and other nearby structures at about $z \sim 1$ because noneuclidean effects are strong only for objects so distant as to be seen when the universe was much younger than it is now. Thus it is useful to study deviations from the standard smooth models to see what the effect of inhomogeneity would be in certain regards and arguably the easiest generalisation of FLRW models, which is also a complete solution of the EFE, is the LTB class of models.

We undertake in chapter 3 an investigation of how the inhomogeneity impacts on observational quantities and its relation to spherical gravitational lensing of light rays. In chapter 4 the possible evolution of density structures in the universe is considered – can overdense

[4]The cosmic X-ray background is also isotropic but only to less than 5%.

[5]It is hoped that the Sunya'ev-Zel'dovich effect – scattering of CMB photons in hot centers of galaxies – might provide a means of testing CH once the technology comes of age within, perhaps, the next five years.

[6]The further back we look down the null cone, the younger the universe is and thus the sources observed will primarily be younger. Young galaxies are still in the violent throes of formation and are thus much brighter than they would be if observed today.

regions evolve into underdensities and if so, under what conditions do they do so, and can density waves occur? Before we deal with these matters in depth we will, in chapter 2, briefly discuss the model's topology and singularity structure and indicate how this has been used to probe our universe theoretically in previous works.

Chapter 2

The Lemaître-Tolman-Bondi Model

And as we stand on the edge of darkness
Let our chant fill the void
That others may know

In the land of the night
The ship of the sun
Is drawn by
The grateful dead.

– Tibetan "Book of the Dead," ca. 4000 BC.

2.1 Close Relatives

It will be illuminating to give some idea as to how and where the LTB solutions fit in with other known solutions of the EFE. Dust solutions of the EFE which satisfy the criteria listed in the introduction are all candidates for describing our universe after recombination. To get an idea of how the LTB model fits in with them and some other solutions, we summarize the classification scheme of Ellis [18] and MacCallum [46].

Clearly, inhomogeneous models with some symmetries must occupy some open set in the space of all solutions. The most popular way of classifying solutions has been to use the

group motions ($G_6 - G_3$) they admit.

- G_6: For a spatially homogeneous perfect fluid with vanishing shear, either the flow is irrotational and thus the space-time is conformally flat (which in the case of a pressureless fluid – 'dust' – means that it is FLRW [37]) or
- G_5: the universe is stationary (the Gödel universe).
- G_4: For a spatially homogeneous perfect fluid dust universe, if the shear and expansion are non-zero, but the vorticity vanishes, a high symmetry class of solutions are the locally rotationally symmetric (LRS) space-times,
- G_3:
  - acting on two-dimensional orbits. We obtain the LTB model, inhomogeneous generalisations of the Kantowski-Sachs model and the plane symmetric Bianchi I model – with 1-dimensional isotropy group.
  - acting on three-dimensional orbits. We obtain the spatially homogeneous Bianchi models (II, VIII and IX) – with 0-dimensional isotropy group.

Recently, a programme has been initiated to classify solutions in a covariant fashion. This has been successful for LRS spacetimes [25]. These classes of spacetimes are characterised by the fact that they have a spatial isotropy at every point (i.e. there is only one preferred spatial direction at every point). The authors used this to split the LRS spacetimes into three categories determined by the twist of the preferred spatial direction and the expansion.

LRS I: a rotating twist- and shear- free family.

LRS II: a nonrotating, twist-free family.

LRS III: a purely twisting homogeneous family.

The class which we are interested in is LRS II: these are inhomogeneous models with a G_3 of isometries. They include hyperbolically symmetric, plane symmetric and spherically symmetric models. The metric takes the form

$$ds^2 = -A(t,r)dt^2 + B(t,r)dtdr + C^2(t,r)dr^2 + R^2(t,r)\left[d\theta^2 + f^2(\theta)d\phi^2\right] \qquad (2.1)$$

where A, B, C and R are functions of t and r only and

$$f(\theta) = \begin{cases} \sinh\theta & \text{hyperbolic symmetry} \\ \theta & \text{plane symmetry} \\ \sin\theta & \text{spherical symmetry} \end{cases}$$

The metric can be diagonalised in the (t,r) plane thus eliminating B (Cf. [69]). For a dust filled cosmology, we usually scale A to 1 thus using synchronous coordinates. Alternatively null coordinates (with $A = C = 0$) may be employed (eg. [34, 47]).

The spherically symmetric solutions are of particular cosmological importance. Solving the vacuum EFE results in the Schwarzschild-Kruskal-Szekeres solution which has one free parameter, the Schwarzschild mass. For a perfect fluid, with given equation of state, the EFE applied to this metric determines the model in terms of essentially two arbitrary functions of r. When the fluid is dust, we can solve the equations of motion exactly and obtain the LTB cosmological models[1].

The model was first discovered by Lemaître [43]. He found the general solution to this cosmology in 1933 [44], obtaining the solutions to the equations of motion for closed models. Tolman (1934) [68], in a study of perturbations away from an FLRW universe, mentions Lemaître's 1933 paper but solved the field equations himself. The model was independently discovered by Datt [13] in 1938. The paper by Bondi (1947) [4] is most often cited. He quotes and solves the field equations completely and also gives the components of the Riemann

[1]Note that it is possible – and in fact has been done many times before – to join various solutions (eg. Schwarzschild to FLRW) to obtain the well-known 'Swiss Cheese' models which are perhaps the closest exact solutions of the field equations to the real lumpy universe.

curvature tensor together with the Kretschmann scalar. Since then, it has been independently rediscovered more than twenty times (Krasiński, 1993 [36] [2]).

2.2 Description

The LTB universe is spherically symmetric, but in general radially inhomogeneous. This means that it is isotropic about one worldline – the centre of symmetry. Space-time is described by a four-dimensional continuum filled by a perfect fluid with a dust equation of state; that is, pressure-free matter. We may choose the natural coordinate system labelled by $\{x^a\}_{a=0}^3 = \{t, r, \theta, \phi\}$ suggested by the spherical symmetry. The coordinates are assumed to be comoving with the particles – the fluid flows along lines of constant spatial coordinate values. This allows a definition of a fluid velocity $u^a = \dfrac{dx^a}{dt}$ in the space-time such that $u^a = \delta^a_0$ and $u_a u^a = -1$, which would mean that time coordinate t is also cosmic time. The flow is irrotational; that is, the vorticity ω_a vanishes.

For an ideal fluid with mass density ρ, pressure p and fluid flow vector u_a

$$T_{ab} = (\rho + p)u_a u_b + g_{ab}p$$

When $p = 0$, the energy-momentum tensor thus has the form

$$T^{ab} = \rho \frac{dx^a}{dt}\frac{dx^b}{dt}. \tag{2.2}$$

The Bianchi identities $G^{ab}{}_{;b} = 0$ via the EFE give rise to the conservation of energy-momentum $T^{ab}{}_{;b} = 0$ with the effect that the dust moves on geodesics;

$$\dot{u}_a = 0 \tag{2.3}$$

which also means that the mass of any portion of the fluid is conserved –

$$\dot{\rho} + \Theta\rho = 0 \tag{2.4}$$

[2]This particular article (to appear as a book) has an extensive list of references on the LTB model.

where the expansion $\Theta = u^a{}_{;a}$.

Consequently we can choose $A = 1$ in (2.1) and the solution pops out when we apply the field equations with a dust source to the metric

$$ds^2 = -dt^2 + C^2(t,r)dr^2 + R^2(t,r)\left[d\theta^2 + \sin^2\theta d\phi^2\right]. \tag{2.5}$$

The field equations are

$$\begin{aligned}
2\frac{\dot{C}\dot{R}}{CR} + \frac{1+\dot{R}^2}{R^2} - \frac{1}{C^2}\left(2\frac{R''}{R} + \frac{R'^2}{R^2} - 2\frac{C'R'}{CR}\right) &= \kappa T^t{}_t = 8\pi G\rho \\
2\frac{\ddot{R}}{R} + \frac{1+\dot{R}^2}{R^2} - \frac{R'^2}{C^2R^2} &= \kappa T^r{}_r = 0 \\
\frac{\ddot{C}}{C} + \frac{\ddot{R}}{R} + \frac{\dot{C}\dot{R}}{CR} - \frac{1}{C^2}\left(\frac{R''}{R} - \frac{C'R'}{CR}\right) &= \kappa T^\theta{}_\theta = \kappa T^\phi{}_\phi = 0 \\
-2\left(\frac{\dot{R}'}{R} - \frac{\dot{C}R'}{CR}\right) &= \kappa T^t{}_r = 0
\end{aligned} \tag{2.6}$$

where the dot indicates differentiation with respect to t and the prime represents differentiation with respect to r. Hereafter, we will use units where $G = 1$.

Upon using the offdiagonal EFE, the metric can be written as

$$ds^2 = -dt^2 + \frac{(R')^2}{1+2E}dr^2 + R^2(d\theta^2 + \sin^2\theta d\phi^2) \tag{2.7}$$

where $R = R(t,r,)$ and $E = E(r)$ is an arbitrary function of the integration. R is the areal radius, that is $4\pi R^2$ describes the surface area of the sphere at comoving radius r at any time t and thus $R(t,r) \geq 0$. R also acts as a transverse scale factor for individual comoving particles.

The expansion Θ is

$$\Theta = \frac{2\dot{R}}{R} + \frac{\dot{R}'}{R'} \tag{2.8}$$

and the shear σ through which the inhomogeneity enters is given by

$$\sigma = \frac{1}{\sqrt{3}}\left(\frac{\dot{R}'}{R'} - \frac{\dot{R}}{R}\right). \tag{2.9}$$

The expression for the invariant energy density, $\rho = \rho(t, r)$, is obtained from the tt field equation:

$$8\pi\rho = \frac{2\,M'}{R^2\,R'} \tag{2.10}$$

where $M = M(r)$ is another arbitrary function.

The rr, $\theta\theta$ and $\phi\phi$ components of the EFE reduce to the single equation of motion

$$\left(\frac{\dot{R}}{R}\right)^2 = \frac{2M}{R^3} + \frac{2E}{R^2}\,. \tag{2.11}$$

This can be solved, even if a non-zero Λ term had been retained, in terms of Weierstrass elliptic functions (see for example [44, 53]). Here where no Λ term is present, the equation of motion has the following solutions in terms of parameter $\eta = \eta(t, r)$.

For a non-empty universe, $M \neq 0$, there are three solutions:

$$R = \frac{M}{2E}(\cosh\eta - 1), \qquad \sinh\eta - \eta = \frac{(2E)^{3/2}(t - t_B)}{M}; \qquad E > 0 \tag{2.12}$$

$$R = \left[\frac{9M}{2}(t - t_B)^2\right]^{1/3}; \qquad E = 0 \tag{2.13}$$

$$R = \frac{M}{(-2E)}(1 - \cos\eta), \qquad \eta - \sin\eta = \frac{(-2E)^{3/2}(t - t_B)}{M}; \qquad E < 0\,. \tag{2.14}$$

When $M = 0$, we have Minkowski space given in either one of two forms:

$$R = (2E)^{1/2}(t - t_B), \qquad E > 0 \tag{2.15}$$

or

$$R = t_B, \qquad E = 0 \tag{2.16}$$

where $t_B = t_B(r)$ is a third arbitrary function. The solutions (2.12), (2.13) and (2.14) have the same evolution as the corresponding FLRW dust solutions , but with spatially variable M, E and t_B. In contrast to the FLRW models, however, it is quite possible to have all three types of evolution in the same model [32]. We will be using the terms closed and open to

describe the topology of the spatial sections and hyperbolic, parabolic and elliptic to describe the time evolution. The late time behaviour of hyperbolic models is given by equation (2.15).

The integration has the result that we have three arbitrary functions of r; $M(r)$, $E(r)$ and $t_B(r)$, which specify the model *up to a radial coordinate freedom.* In other words, there are two physically independent arbitrary functions, plus a freedom to rescale the r coordinate. These functions also have a physical meaning and are not completely arbitrary.

The function $t_B(r)$ is the time of the Big Bang in all models and determines the time of the Big Crunch in elliptic sections[3]. The bang surface thus need not be a surface of simultaneity – it occurs at different times for different observers as determined by t_B. The gradient of t_B generates the decaying modes of the perturbation to an FLRW background [63].

$M(r)$ is the effective gravitational mass within r and can be defined by a component of the Riemann tensor [28];

$$\frac{2M}{R} = R^{\phi}{}_{\theta\phi\theta}\,.$$

We assume that $M \geq 0$ ($M < 0$ implies negative mass). Integration of equation (2.10) on a constant t surface yields

$$M = 4\pi \int_0^r \rho R^2 R' dr\,. \tag{2.17}$$

This differs from the integral of ρ with respect to the volume element on constant t surfaces

$$\overline{M} = 4\pi \int_0^r \rho \frac{R^2 R'}{\sqrt{1+2E}}\, dr \tag{2.18}$$

which difference one may attribute to the energy of the gravitational field contributing to the net gravitational mass.

The local geometry is determined by $E(r)$; i.e locally hyperbolic, parabolic and elliptic regions occur when $E(r) > 0$, $E(r) = 0$ and $E(r) < 0$ respectively. If we compare equation

[3]The bang surface is spacelike, except for the single central point which may have a shell focusing singularity on the bang or crunch.

(2.11) with the Newtonian analogue of a dust cloud we see that E acts as an energy potential: for an infinitesimal shell between r and $r+dr$, E is the sum of the kinetic and potential energy per unit mass of the shell. (Cf. [3, 52]). Its gradient generates the growing modes of the perturbation to an FLRW background [63]. We shall assume that our spacetime does not change its signature, thus from equation (2.7) we must have $E(r) \geq -\frac{1}{2}$ $(\forall r)$.

The following result also holds [32] in two of the non-trivial solutions by eliminating η in (2.12) and (2.14):

$$\frac{R'}{R} = \left(\frac{M'}{M} - \frac{E'}{E}\right) - \left\{t_B{}' - \left(\frac{3E'}{2E} - \frac{M'}{M}\right)(t - t_B)\right\}\frac{\dot{R}}{R}. \tag{2.19}$$

The corresponding equation for (2.13) is obtained by setting $E' / E = 0$ in the above.

2.2.1 The Friedmann-Lemaître-Robertson-Walker limit

In the homogeneous FLRW case – $\rho = \rho(t)$ only – the requirement that η be independent of r at all times in (2.12) and (2.14) implies that

$$t_B = \text{constant}, \qquad M \propto |E|^{3/2}. \tag{2.20}$$

For an FLRW universe, $R = a(t)\tilde{a}(r)$ gives the FLRW scale factor, $a(t)$, when the radial coordinate is chosen as $\tilde{a}(r) = r$ and $2E(r) = -kr^2$ in the standard way[4]. The RW metric that results then is

$$ds^2 = -dt^2 + a^2(t)\left[\frac{dr^2}{1-kr^2} + r^2\left(d\theta^2 + \sin^2\theta d\phi^2\right)\right], \tag{2.21}$$

where k is an arbitrary constant determining the curvature of the t = constant spatial sections;

$k > 0$ – the spatial sections have a constant positive curvature.

$k = 0$ – the spatial sections are flat.

$k < 0$ – the spatial sections have a constant negative curvature.

[4]Another common choice is $2E(r) = -\sin^2 r$ or $2E(r) = -\sinh^2 r$ for the $k = +1$ and $k = -1$ cases respectively.

Because the density is spatially homogeneous, equation (2.17) gives

$$M = \frac{4\pi}{3}\rho R^3$$

as expected.

Of course, we could alternatively obtain the (dust) FLRW models as a limit of the LTB models by letting the shear vanish in (2.9).

The FLRW limit also appears in the limit as $t \to \infty$ for parabolic and hyperbolic models which have their inhomogeneity specified fully by $t_B(r)$ [5]. In fact, all parabolic models tend to the Einstein-de Sitter model at late times and the hyperbolic models tend to the FLRW case provided a given condition on the arbitrary functions is satisfied[5].

2.2.2 Behaviour at the Origin

An origin occurs at r_0 when $R(t, r = r_0) = 0$ for all t. We can assume $r_0 = 0$ without loss of generality and shall adhere to this choice throughout this piece of work. For a sphere centred around $r = 0$, $R(t, 0) = 0\,(\forall t)$ and $R(t, r) \geq 0\,(\forall t\,, r > 0)$ with the equality occurring on the bang and crunch.

We may have cases with one origin as in open and marginally open models [6]. A closed model has $R'(t, r \to 0) > 0$ and at the other centre $r = r_\infty$ we have $R'(t, r \to r_\infty) < 0$ [7] as pointed out by Zel'dovich and Grischuk [74].

We note the following behaviour of the arbitrary functions at the origin of coordinates.

As previously stated, a spatial origin occurs if $R(t, 0) = 0$. Thus, from equation (2.12) or equation (2.14), it is clear that $R(\eta(t, r = 0), r = 0) = 0 \;\; \forall \eta > 0$ requires

$$\left.\frac{M}{E}\right|_{r \to 0} \to 0 \tag{2.22}$$

[5] For elliptic models the late time behaviour is still dependent on the initial inhomogeneity created by the nonsimultaneous bangtime surface and thus will not be FLRW (where the crunch is simultaneous). However if the inhomogeneities are small enough at the start, the crunch can be made to be nearly smooth.

[6] There exist models with no origin: for example you may have two different spacetime regions connected to each other by a 'Schwarzschild throat' as demonstrated by Hellaby [29].

[7] considering the coordinate r to be affine here.

provided we are away from the bang ($\eta = 0$) or crunch ($\eta = 2\pi$ in elliptic models). Alternatively, we could say that $RE\,/\,M$ is finite here; that is,

$$\left.\frac{2RE}{M}\right|_{r\to 0} = \phi_0, \tag{2.23}$$

where ϕ_0 is a nonzero and finite (except on the bang or crunch) function of η whose functional form is given on the left hand side of (4.4).

We recall the equation of motion which holds in all three LTB models, namely equation (2.11). We want our origin to remain an origin for all times (meaning no change of topology is allowed) – that is to say $\dot{R}(t,0) = 0$, $(\forall t)$. This tells us that

$$E|_{r\to 0} \to 0 \text{ and } M|_{r\to 0} \to 0 \tag{2.24}$$

separately. This finding is quite compatible with the fact that we have an FLRW-like origin and does not necessarily mean that we have parabolic evolution at the origin. Indeed, it would be more accurate to define the applicable solution (2.12) - (2.14) by the sign of $E^{3/2}/M$ or RE/M instead of E [30].

Furthermore, we require the evolution rate to be finite for $t > t_B$. More specifically, the function $t(\eta, r = \text{constant})$ should not change radically as $r \to 0$. Thus $\exists$ finite, nonzero ξ – a function of η – such that

$$\left.\frac{(2E)^{3/2}(t - t_B)}{M}\right|_{r\to 0} = \xi\,. \tag{2.25}$$

ξ is defined by the right hand side of (4.4). Since M and $2E$ both vanish near the origin, the above condition in conjunction with (2.24) tells us that $M \propto E^{3/2}$ to lowest order in r which is the case globally in a Robertson-Walker (FLRW) model.

Given that $RE/M|_{r\to 0}$ is finite and $\left.E^{3/2}/M\right|_{r\to 0}$ is finite, we can deduce that near $r = 0$

$$E \sim R^2 \text{ and } M \sim R^3 \tag{2.26}$$

on a constant time slice.

We assume the density, given by equation (2.10), to be positive and finite away from the bang and crunch. Thus

$$0 < \frac{M'}{R^2\, R'} < \infty \tag{2.27}$$

which is consistent with $M \sim R^3$ near $r = 0$. Zero density at the origin would require the Minkowski space evolution (2.15) there. But this scenario describes a set of measure zero in the set of all LTB models and we do not consider it further here.

There must be no curvature singularities at the origin. This is often associated with the fact that a scalar quantity like the Kretschman scalar remains finite[8]. The Kretschman scalar, K, in the LTB model is given by

$$K \equiv R^{abcd} R_{abcd} = 48 \left(\frac{M}{R^3}\right)^2 - 16 \frac{M}{R^3} \left(\frac{2\, M'}{R^2 R'}\right) + 3 \left(\frac{2\, M'}{R^2 R'}\right)^2 \tag{2.28}$$

where R^{abcd} is the Riemann tensor. So to forbid curvature singularities at the origin, the 'mean density' term $\dfrac{M}{R^3}$ must be finite; that is,

$$\frac{M}{R^3} < \infty\,. \tag{2.29}$$

Again, since $M \sim R^3$, we have that $K(t, r = 0) \neq 0$.

The above discussion can be summarised as follows. Away from the bang or crunch surfaces as $r \to 0$ in non-empty LTB models,

$R \to 0$, $\dot{R} \to 0$, $E \propto R^2 \to 0$, $M \propto R^3 \to 0$ and

$\rho \to \rho_0(t), \quad 0 < \rho_0 < \infty$

$K \to K_0(t), \quad 0 < K_0 < \infty.$

2.3 Singularities

The Hawking-Penrose Singularity Theorems [27] (1970) showed, that under very general conditions, GR results in space-time singularities of a gravitational nature. All expanding,

[8] but see also the discussion in section 2.3.

physically reasonable cosmological exact solutions of the EFE have space-time singularities. Intuitively, one would consider a singularity to be an event where the curvature of space-time diverges. The problem is that, unlike other physical theories, GR does not assume any underlying fixed metric structure for a physical event. We actually have to solve *for* the space-time metric itself and once we have done this, we find that singular points are outside the spacetime. Thus we cannot assign a location in space or time to a singularity and the EFE does not hold there.

One way of locating a singularity is to use the fact that the curvature in a parallelly propagated frame becomes unbounded there. Of course, if we use the criterion that one (or maybe more) of the components of $R_{abc}{}^{d}$ runs off to infinity in an arbitrary basis, this would be insufficient since the bad behaviour could just be due to a bad coordinate base. An attempt to circumvent this problem is to use scalars formed out of the curvature tensor like the Ricci scalar $R = R_{ab}\,R^{ab}$ or the Kretschmann scalar, K, but this does not work in a spacetime with indefinite signature. In particular, the solutions of the field equations describing colliding plane waves have vanishing curvature scalars, but singular $R_{abc}{}^{d}$ [26]. Thus nowadays it is widely accepted that geodesic incompleteness characterises a singularity.

However, if the universe did contain singularities we would expect them to occur in essentially three places:

- The Big Bang;
- The Big Crunch (if it should take place);
- Gravitational collapse of a massive body.

In the LTB model, in addition to the usual bang singularity (and crunch singularity in elliptic models), we also have two other regions where the EFE do not hold. We have shell crossing singularities occurring, typified by $R' = 0$ and $R \neq 0$, and shell focussing singular-

ities where $R' = 0$ and $R = 0$ at the centre of a collapsing dust cloud.

2.3.1 Shell Crossings

Loosely stated, a shell crossing occurs when an inner spherical shell of matter moves faster than an outer shell and eventually bursts through. A locus of points is formed where $R' = 0$ and $R \neq 0$. This was described by Yodzis et al [73]. Since the Kretschmann scalar diverges, one may naturally consider this to be a 'true' singularity. It should be mentioned, however, that Clarke [10][9] has demonstrated a way of extending the spacetime through a shell crossing singularity.

This singularity is different to the Big Bang and Big Crunch mathematically and physically. Firstly, at a shell crossing we only have one metric component in equation (2.7) going to zero (g_{rr}); and the singular surface is timelike. The light coming from a shell crossing is finitely red or blue shifted and the surface density on the intrinsic metric induced by $R' = 0$ obeys the 'strong energy condition' on this surface [31, 39].

It has long been argued whether this singularity is physical or whether it just represents a breakdown of the fluid assumption. Weinberg claims in his book [71] that non-zero pressure would remove this feature. However, Müller zum Hagen et al. [73] have displayed spherically symmetric models with pressure which have shell crossings. Hellaby and Lake also show in the appendix to their 1985 paper [32] that the physical attributes of a shell crossing hold for spherically symmetric models regardless of equation of state.

To eliminate the occurrence of shell crossings it is sufficient to assume $R' > 0$ and $M' > 0$. In fact this has often been done (for example [41]). However, these conditions are too restrictive. In a closed model, they exclude the regular maxima which must occur at $R' = 0$. Regular extrema along a constant time slice, instead of shell crossings, may occur provided the density ρ remains finite at that point. By using equation (2.10) and equation (2.19),

[9] See also Kriele [38] and references therein.

$E \geq 0$	$E < 0$
$R' > 0$	
$t'_B \leq 0$ $E' \geq 0$ $M' \geq 0$ but no more than two equalities at once.	$t'_B \leq 0$ $t'_B \geq \frac{-\pi M}{(-2E)^{3/2}}\left(\frac{M'}{M} - \frac{3E'}{2E}\right)$ $M' \geq 0$ but not both $M' = 0$ and $E' = 0$ at once.
$R' = 0$	
$t'_B = 0$ $E' = 0$ $M' = 0$	$t'_B = 0$ $E' = 0$ $M' = 0$
$R' < 0$	
$t'_B \geq 0$ $E' \leq 0$ $M' \leq 0$ but no more than two equalities at once.	$t'_B \geq 0$ $t'_B \leq \frac{-\pi M}{(-2E)^{3/2}}\left(\frac{M'}{M} - \frac{3E'}{2E}\right)$ $M' \leq 0$ but not both $M' = 0$ and $E' = 0$ at once.

Table 2.1: The Conditions for No Shell Crossings.

Hellaby and Lake showed that the conditions under which this occurs do not specifically require $1 + 2E = 0$[10] as previously thought, but only that

$$M' = 0, \quad E' = 0, \quad \text{and} \quad t'_B = 0\,. \tag{2.30}$$

The necessary and sufficient conditions under which shell crossings do not occur[11] were derived by Hellaby and Lake [32]. They are summarised in Table 2.1.

The above considerations seek to exclude the occurrence of shell crossings (or shocks). Mészáros [50] defines a shell crossing in a way which allows one to determine the time of shell crossing. He then uses them to describe a process of galaxy formation. Other authors have continued this line of research using them as a mechanism for structure formation since their occurrence leads to a sudden density excess (see for example [52]) and have been successful in describing many observed structures on virtually all scales. This will be further discussed

[10]When $1 + 2E \neq 0$, then a surface layer of matter occurs.

[11]A similar result for the more general quasispherical Szekeres model is given in [66].

in chapter 4.

2.3.1.1 Curvature Change

The topology of the spatial sections is something which is usually treated only in the simplest cases in classical cosmology. It has been shown that in the FLRW-models, topology change is not possible. In particular, models with hyperbolic geometry (and with $\Lambda = 0$) are always expanding and likewise, elliptic models always recollapse.

However, Hellaby and Lake [31] showed that this is an unstable situation since certain radial perturbations (that is LTB models) exist which are locally open (with $\Lambda = 0$) and recollapse.

In 1978, Papapetrou [55] showed that a closed model can exist within a parabolic exterior. Zel'dovich and Grischuk in 1984 put forward the hypothesis that a globally closed world must recollapse everywhere. The mechanism by which this occurs would be through the streaming of particles through caustics which closes up the hyperbolic region. This was backed up by Bonnor (1985) [6] who provided a proof subject to some stringent conditions on E: E must decrease from zero at the origin and all its derivatives which are nonzero at the origin must be continuous[12].

Hellaby and Lake produced models where this hypothesis breaks down[13]. These models had no shell crossings and thus no streaming of matter could occur into open regions. They also pointed out that the restriction Zel'dovich and Grischuk had on E forces the model to collapse and thus provided their result. It turns out that, given the conditions for no shell crossings tabled above, this constraint is not necessary for physically reasonable models[14].

Observations suggest [11] that $\Omega < 1$, but this does not mean that the universe necessarily would expand forever. Specifically, we note that at small scales Ω is found to be small and

[12]Of course, E must also not be less than $-\frac{1}{2}$ for the spacetime to remain Lorentzian.
[13]although their closed hyperbolic model included a surface layer.
[14]For a more recent treatment, consult [8].

then systematically increases with larger observational scales. This could conceivably be due to us being in a locally hyperbolic region embedded in a globally flat (or elliptic) LTB model.

2.3.1.2 LTB and silent universes

The silent universes [49] are so called because the ten nonlinear partial differential EFE (1.1) reduce to a coupled set of *ordinary* differential equations (ODE's). This reduction is very significant since it makes the evolution of each worldline decouple (which implies that information is not passed from one to the other and hence the name 'silent universe') and the numerical evolution becomes much simpler to study, as is the study of their generic endpoints of gravitational collapse. This reduction is possible because the assumptions $p = H_{ab} = 0$ are imposed on the fluid flow, where H_{ab} is the magnetic part of the Weyl tensor. If in addition, we impose the restriction $\omega_a = 0$, where ω_a is the vorticity vector, then the shear tensor, electric part of the Weyl tensor and the metric become simultaneously diagonalisable, and the coupled set of ODE's is only six dimensional. This set describes *exactly* the flow in the linear and nonlinear regimes and is thus useful for discussing structure formation.

Since the LTB model is also dust ($p = 0$), the flow is irrotational ($\omega_a = 0$), and it can be shown that $H_{ab} = 0$, it follows that the LTB model is a silent universe [24].

It is interesting to note that shell crossings, where the $1 - 1$ nature of the Lagrangian flow breaks down (caustic formation in the language of catastrophe theory), typified by the Zel'dovich pancake solution, occur in both the LTB and silent universes.

2.3.2 The Shell Focussing Singularity

The other nonstandard singularity that occurs in the LTB model is the shell focussing singularity – also known as the ESC singularity[15] – which occurs at the intersection of the origin with the bang and crunch surfaces. It was found that for some models, first of all, an initial

[15]First discovered by Eardley and Smarr [17] in a numerical study of a parabolic collapsing model in 1978 and later investigated in a mathematical study of an elliptic model by Christodoulou (1984) [9].

ray can emerge from the final singularity; and secondly, this ray could escape to infinity – in addition, whole families of light rays can do so. Thus this singularity is of considerable interest since there are a wide range of LTB models for which it is naked and gravitationally strong – allowing no extension of the incomplete geodesics through it – and thus produces counterexamples to the well-known Cosmic Censorship Hypothesis which asserts that the endpoint of gravitational collapse is a 'clothed singularity'. Obviously, this is a topic which is under great discussion still, but it is also a rather specialised topic which would require considerable detail and background information if we were to attempt to discuss it here in all its complexity. We deem this too much of a digression and refer the reader to the excellent review article by Clarke [10] for further references and what the current verdict is on this major problem in Relativity.

Chapter 3

Effect of Radial Lensing on Distance Measurements

"Well," Brahma said, "even after ten thousand explanations, a fool is no wiser, but an intelligent man requires only two thousand five hundred."

– The Mahabharata.

Before getting into this issue in depth, we need to provide some background information on Gravitational Lensing.

3.1 Gravitational Lensing

We may define lensing to be the distortion of the path of light rays in a general inhomogeneous (lumpy) universe so that the light ray path is different from what it would have been without the inhomogeneity. Since after Newton, it was suggested that the effect of gravity would result in a bending of light. A landmark verification of GR was the measurement of the deflection angle of light by the gravitational field of the sun which was measured to be twice that of the Newtonian result as predicted by GR. This may be considered to be the first lensing system ever studied. Since then, the topic of gravitational lensing has become more sophisticated and is currently under a great amount of research after the discovery in 1979

of the first lensed galaxy 0957+561 in a radio survey[1], which had a redshift of $z \sim 1.4$ [70].

In a general curved spacetime, plane waves do not exist. However, in a normal lensing situation, the wavefronts observed may be plane on a scale (large compared with wavelength) which is negligible compared to the curvature of spacetime. These wavefronts may be represented by the WKB approximation to Maxwells equations. The wavefronts are constant phase hypersurfaces and the corresponding wavevectors k_a are the characteristics of Maxwells equations which can be shown to be tangent to the local light cone; and in this approximation the light rays are null geodesics.

3.1.1 Strong and Weak Lensing

In a general universe, the future-directed null geodesics from a luminous object form a smooth bundle initially near to the object. Due to lensing, these null geodesics may develop sheets which intersect each other resulting in multiple images of that object (as has been observed in many lensing situations). Loosely stated, the locus of self-intersection of sheets where the expansion or shear diverges is called the caustic of the light cone. The magnification of a source (in the geometric optics limit) becomes infinite as it approaches a caustic. Of course, at these points, the geometrical optics limit breaks down since the wavefronts detected by the observer may be then in principle mutually coherent and this implies that wave optics should be used; that is interference effects are relevant. For most lensing situations, however, wave effects are fairly negligible because the typical sources are not compact enough (Cf. [61]).

In addition to the deflection of light, gravitational lensing also affects the flux of the image of a source since the cross-sectional area of a light bundle is distorted. This results in a magnification of the source given by the ratio of observed flux to undeflected flux which, because of photon conservation, is equal to the ratio of observed solid angle to its original unlensed solid angle subtended in the sky.

[1]The lensing galaxy was discovered later at a redshift of $z \sim 0.36$.

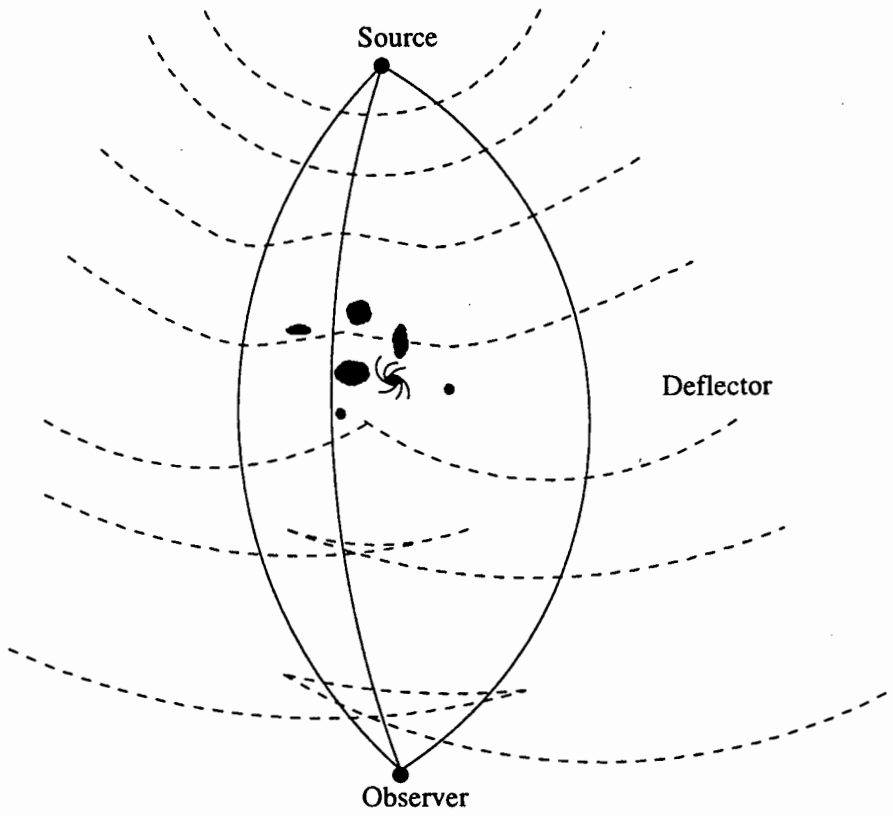

Figure 3.1: (Adapted from [61].) The wavefronts in a typical lensing system. Close to the source the wavefronts (dashed lines) are nearly spherical, but as they approach the deflector, they become deformed and may self-intersect forming caustics. Every passage of the wavefront past the observer corresponds to an image of the source in the direction of the light rays (solid lines), perpendicular to the wavefront. This illustrates the well known theorem that an odd number of images of a source are detected for a multisheeted wavefront. For radial lensing there is no bending of the wavefront at all; only a uniform early or late arrival of the wavefronts, when compared with a smooth model, occurs.

Weak lensing implies a change of apparent positions and luminosities and alteration in the usual distance relations, usually combined with image distortions, but not multiple imaging. It has been used successfully to trace mass distributions in clusters and galaxies using the fact that light bends due to both luminous and dark matter[2]. The impact of weak lensing (and to a much lesser extent, strong lensing) on the CMB has recently become a topic of investigation (eg. [62]).

Speaking very loosely, we can draw the following distinction between weak and strong lensing. In a universe which is composed of clumps separated by large 'empty' regions, strong lensing occurs for those light rays which are within the critical distance of a lensing object which has sufficient gravitating mass to cause multi-sheeting of the wavefronts. Weak lensing occurs for those light rays which pass far away enough from the clumps to not be bent enough to let caustics form before being observed.

Ellis, Bassett and Dunsby [20] argued that the Dyer-Roeder distance [15][3] is generally regarded as a good approximation for ray bundles moving between high-density clusters of matter, resulting in a de-focussing relative to the comparable FL model, but matter moving near or through higher density regions is more focused than in the FL model, so resulting in a compensating effect. It is commonly believed [72, 61] that an exact cancellation between the two effects takes place when one averages over large angular scales containing both high and low density regions – so the FL area distance is the correct one on these scales. However, it was pointed out in [20] that, after caustics have formed through the focussing of light rays by the high density regions, these light rays too are rapidly diverging so that sufficiently far down the past light cone *all* light rays will be diverging relative to the comparable FL model. Consequently there is good reason to believe the general opinion in this matter is wrong; that

[2]It is sensitive enough to have detected a 'brown dwarf'-like object in the Large Magellanic Cloud.

[3]The Dyer-Roeder distance formula gives the area of a bundle of light rays against redshift as a differential equation as if those rays were travelling in an FL model with lower density. This density is determined by how much of the universe can be taken to be in clumps.

in fact 'shrinking' takes place.[4]

It is often argued that photon conservation excludes this possibility [72], but these arguments are based on incorrect assumptions about the geometry. The point is that we have an inhomogeneous universe, which has nonlinear density fluctuations at some scales and we allow radiation (the CMB for example) to propagate through it and to possibly even develop multisheeted caustics. We then average that *wavefront* to find the total area and hence the average area distance to that redshift. The question is then to compare it with the wavefront obtained by smoothing the *geometry* of the spacetime of the inhomogeneous universe and allowing the CMB to propagate through the smooth geometry. It is not at all apparent that these two measurements should be the same. Moreover, even when there is only weak lensing, and caustics have not formed, it is not obvious that the FL area distance-redshift relation is an accurate description.

Included in these weak lensing situations, we may consider the very simple case of *radial lensing* which is a spherically symmetric distortion of the null cone compared with a (homogeneous) FL model, caused by a spherically symmetric mass distribution around the origin, resulting in a uniform delay of the wavefront relative to a homogeneous cosmology. There is no image distortion, no dependence of magnification or time delay on direction, and no multiple imaging, but we will here show that its effects are significant. The situation is analogous to observing a spherically symmetric wavefront emanating from the centre of a glass sphere which has regions of differentially increasing and decreasing optical index and comparing areas of wavefronts to that obtained by passing the light through a glass sphere of uniform optical index. The wavefront that passes through a relatively denser area, say,

[4]The term shrinking [45] describes the following. If at some redshift the area distance is greater in the inhomogeneous universe than in the best-fit or background FL model, scales at that redshift will be underestimated if the FL area distance is used to calculate the size of objects from their measured angular size, and so will have 'shrunk' relative to their actual scales in the more realistic model. Put another way, if a sphere at given z about the observer has a larger total area in the inhomogeneous model, an object of fixed size will subtend a smaller solid angle on the sky, and so be shrunk. (See [20] for more discussion.)

will be slowed down with the result that when we compare its size to those of wavefronts in the smooth sphere, it will seem to fit a wavefront in the smooth sphere at an earlier point (relative to the point chosen in the denser area in the inhomogeneous sphere). Thus the wavefronts in the dense area appear as if they are of greater optical depth and thus of smaller size; hence this can legitimately be regarded as lensing.[5]

3.2 Shrinking and Magnification Caused by Radial Lensing

Our aim here is to show that when analyzing observations at large redshift in the real universe, the assumption of an area distance corresponding to that of a best-fit Friedmann- Lemaître (FL) model – that is, one with a matching averaged matter density – may not be a good approximation, even when averaging over large angular scales. This claim [72] is important because of the ubiquitous use of FL models in studies of number counts and the cosmic microwave background. It demonstrates the existence of radial lensing effects.

We shall construct an exact inhomogeneous model and its FL approximation, and compare the area distance-redshift and density-redshift relations in the two. To do so we examine Lemaître-Tolman-Bondi (LTB) spherically symmetric dust solutions, where exact integrations of the field equations are available for the past light cone of observers at the central position. Although the lensing that occurs for this central observer is purely radial, we find the inhomogeneity has a tangible effect on observational relations. In the particular case examined, because of the spherical symmetry about the observer, the effect in any specific direction will not be compensated by an opposite effect in another direction - on the contrary, the effect is uniform because it is the same in all directions, and will occur on large as well as small angular scales. However unlike the aforementioned paper [20], this will not be associated

[5]To extend this analogy to the real universe, we may consider the sphere to be not just of differential optical density, but as made up of bubbles of overdensities in a low density medium.

with the formation of caustics.

The failure of the FL-like area distance-redshift assumption will thus have been shown to occur for observers at a very special position in a family of high-symmetry space-times. Undoubtedly this is not the kind of situation the authors of the papers mentioned above, claiming the effect does not occur [72, 61], had in mind. However the usual statements of this effect contain no clauses that exclude this situation: the result is supposed to hold in all cases when the 'lumpy' universe is reasonably close to an FL model, and observations are averaged over the sky; their arguments do not exclude the situation envisaged here where the observer is at the centre of a spherically symmetric inhomogeneity. Indeed, a spherically symmetric model may be regarded as describing data that has been averaged over the *whole* sky, but not over distance.

Our example thus confirms the claims of paper [20], in the setting of particular exact inhomogeneous solutions of the Einstein Field Equations. It does not generically establish the magnitude of the effect, precisely because the high-symmetry geometry considered here precludes formation of caustics and the consequent fractal-like structure of the real light cone.

In developing the results of this section we solve one of the major problems that has made analysis of observations in Lemaître-Tolman-Bondi solutions difficult, namely the problem of precisely locating the past light cone of the chosen central event $\mathrm{P} = (t_0, 0)$, by use of a special choice of radial coordinate that ensures a very simple form for the past light cone of P in these inhomogeneous space-times. This technical development has other uses in terms of analysing observational relations in these models.[6]

[6]For a slightly different analysis of LTB spacetimes, based on null cone coordinates, see [47], and for a consideration of observations away from the centre of symmetry see [34].

3.2.1 Programme

The question we are raising is whether the area of an averaged wavefront we receive at our observatory in an inhomogeneous universe is the same as the area of a wavefront in a smoothed version of that universe. To clarify this issue our strategy is to:

- Select (arguably) the most natural generalisation of the Einstein-de Sitter models commonly used in studies of observations – a parabolic LTB model – and describe data on the null cone.
- Find the FL limit of this inhomogeneous universe in an appropriate coordinate system.
- Average the lumpy universe in a natural way and fit it correctly to an FL model.
- Compare area distances in the lumpy universe and its smoothed average.

3.2.1.1 The Inhomogeneous Model

The Integrated Field Equations We choose the parabolic LTB model which is perhaps the natural generalisation of the $\Omega = 1$ dust FL model. This model is characterised by the mass within comoving radius r, $M(r)$, and the 'bang-time' function $t_B(r)$ describing the locus of the initial spatial hypersurface (that is, the local time of the big bang). The two arbitrary functions represent a physical freedom and a coordinate freedom, e.g. $t_B(M)$ and $M(r)$, respectively (Cf. section 2.2).

In normalised comoving coordinates the metric after solving the off- diagonal EFE is

$$ds^2 = -dt^2 + (R')^2 dr^2 + R^2(d\theta^2 + \sin^2\theta d\phi^2)\,. \tag{3.1}$$

The spatial sections are flat because if, for an arbitrary time t_0, we choose $r = R(t_0, r)$ then $R'(t_0, r) = 1$ and we find that the 3-spaces have metric $d\sigma^2 = dr^2 + r^2 d\Omega^2$ and hence are clearly flat.

In the parabolic case R is given explicitly by the solution to the equation of motion

$$\dot{R}(t,r) = \sqrt{\frac{M(r)}{R(t,r)}} \tag{3.2}$$

obtained from the rr, $\theta\theta$ and $\phi\phi$ components of the EFE as before ; that is

$$R(t,r) = \left[\frac{9M(r)}{2}(t - t_B(r))^2\right]^{1/3} \tag{3.3}$$

where t is cosmic time whilst M and t_B are both functions of coordinate radius r only. It follows immediately that

$$R'(t,r) = \frac{3}{2R^2(t,r)}\left[M'(r)(t - t_B(r))^2 - 2M(r)(t - t_B(r))t'_B(r)\right] . \tag{3.4}$$

The tt field equation gives the density

$$4\pi\rho(t,r) = \frac{M'(r)}{R^2(t,r)R'(t,r)} . \tag{3.5}$$

as before.

The Solution on the Null Cone Since we are interested in observations on the null cone we must project onto it by specifying the unique relationship between r and t. The radial null trajectories are given by $ds^2 = 0 = d\theta^2 = d\phi^2$, and since they are unique are thus radial null geodesics. So from (3.1), if the past light cone of the event $(t = t_0, r = 0)$ is given by $t = \hat{t}(r)$, then that light cone is described by

$$dt = \pm R'(\hat{t}(r), r)dr . \tag{3.6}$$

The coordinate freedom in the LTB metric is a rescaling of the radial coordinate $r \to \tilde{r} = \tilde{r}(r)$. If we choose r so that

$$R'(\hat{t}(r), r) = 1 , \tag{3.7}$$

then on the past light cone $dt = -dr$, so that the incoming light rays at the event $(t = t_0, r = 0)$ are given by

$$\hat{t}(r) = t_0 - r . \tag{3.8}$$

So this gauge choice, in contrast to other work done on observations in the LTB model, locates the null cone of the observer at one instant of time, in its simplest possible form, and makes

our programme analytically solvable[7]. On this light cone, putting (3.8) in (3.4) and using (3.7),

$$R'(\hat{t}(r),r) = \frac{3}{2R^2(\hat{t}(r),r)}[M'(r)\tau(r)^2 + 2M(r)\tau(r)\tau'(r) + 2M(r)\tau(r)] = 1 \tag{3.9}$$

where we have defined

$$\tau(r) = t_0 - r - t_B(r)\,. \tag{3.10}$$

The function $\tau(r)$ can be interpreted as proper time from the bang surface to our past null cone along the particle worldlines. We can set t_0 to be the time since the bang at the observer ($r = 0$) by choosing $t_B(0) = 0$ (so $\tau(0) = t_0$).

It is important to realise that evaluating $R'(t,r)$ on the null cone $t = \hat{t}(r)$ is not the same as differentiating $\hat{R}(r) = R(\hat{t}(r),r)$ with respect to r. In fact, by evaluating (3.3) on the null cone, $\hat{R}$ is given by

$$\hat{R} = R(\hat{t}(r),r) = \left[\frac{9M(r)}{2}\tau(r)^2\right]^{1/3} \tag{3.11}$$

which means that its derivative is given by

$$\frac{d\hat{R}}{dr} = \frac{d}{dr}[R(\hat{t}(r),r)] = \frac{3}{2R^2(\hat{t}(r),r)}[M'(r)\tau(r)^2 + 2M(r)\tau(r)\tau'(r)]\,. \tag{3.12}$$

The areal radius when evaluated on $\hat{t}(r)$, $\hat{R} = R(\hat{t}(r),r)$, at time t_0 in the Lemaître-Tolman-Bondi metric, is the area of the intersection of our past null cone $(t_0,0)$ with past spacelike time surfaces (in this case spheres) so it is the *area distance*. Combining the above equation (3.12) with the choice (3.9) gives a first order differential equation for $\hat{R}$.

$$\frac{d\hat{R}(r)}{dr} + \frac{3M(r)\tau(r)}{\hat{R}(r)^2} = 1\,. \tag{3.13}$$

In summary, with our choice of coordinates we have recast the flat LTB model in a form that allows us to locate the past null cone of $t = t_0, r = 0$ with ease. This has left us with

[7]If there are conformal Killing vectors in the spacetime, one can solve for the null geodesic tangent vectors algebraically (in perhaps the more traditional fashion).

one physical freedom to choose an arbitrary function of r. We could choose τ (or M) and substitute (3.11) into (3.13). Solution of this differential equation would determine $\hat{R}$ and thus any other quantity. If we instead decide to choose $\hat{R}$, that is, the area of the wavefront, then the model is trivially and fully specified by (3.11) and (3.13). It follows that

$$\tau(r) = \frac{2\hat{R}(r)}{3} \Big/ \left(1 - \frac{d\hat{R}(r)}{dr}\right) \tag{3.14}$$

and

$$M(r) = \frac{\hat{R}(r)}{2}\left(1 - \frac{d\hat{R}(r)}{dr}\right)^2 \qquad (M(0) = 0)\,. \tag{3.15}$$

To obtain the results of the next section, we will fix the geometry by choosing $\hat{R}$. This will then determine $\tau(r)$ (equivalently $t_B(r)$) and $M(r)$ by the above two equations. The flat LTB model will thus be fully specified in these coordinates and one could then propagate the data off the null cone numerically by the comoving assumption if needs be.

The density on the null cone $\hat{\rho}(r)$ is found by evaluating (3.5) on the null cone:

$$4\pi\hat{\rho}(r) = \frac{M'(r)}{\hat{R}(r)^2} \tag{3.16}$$

and its value at the origin depends on the time as characterised by the Hubble constant;[8]

$$\Omega = \frac{4\pi\rho}{H^2} = 1 \quad \Rightarrow \quad \rho_0 = \frac{H_0^2}{4\pi}, \quad t_0 = \frac{2}{3H_0}\,. \tag{3.17}$$

Redshifts It is of some importance that we state the relevant quantities in terms of redshifts. To do this, we use the fact that in the geometric optics limit, for two light rays emitted on the worldline at r_{em} with time interval $\delta t_{em} = t^+(r_{em}) - t^-(r_{em})$ and observed on the central worldline with time interval $\delta t_{ob} = t^+(0) - t^-(0)$

$$1 + z = \frac{\delta t_{ob}}{\delta t_{em}}\,. \tag{3.18}$$

[8]Since measurements of the Hubble constant are taken at about $z < 1$, we can take this to determine the age of the universe, t_0, at the central observer.

The past radial null geodesics are given by

$$dt = -R'(t,r)dr\,,$$

so for an observer on a nearby worldline, the time interval changes by

$$d(\delta t) \;=\; dt^+ - dt^- \;=\; \left[R'(t^-,r) - R'(t^+,r)\right]dr \;=\; -\frac{\partial}{\partial t}\left[R'(t,r)\right]\delta t dr\,.$$

Thus

$$d\ln\delta t = -\frac{\partial}{\partial t}\left[R'(t,r)\right]dr$$

which means that the redshift, given by (3.18), is

$$\ln(1+z) = \int_0^{r_{em}} \dot{R}'(\hat{t},r)dr \tag{3.19}$$

where $\hat{t}(r)$ is the equation of the null cone.[9] To calculate $\dot{R}'(t,r)$ we differentiate (3.4) with respect to t

$$\dot{R}' = \frac{\dot{R}}{3}\left[\frac{t_B'}{t-t_B} + \frac{M'}{M}\right], \qquad \dot{R} = \left[\frac{4M}{3(t-t_B)}\right]^{1/3}. \tag{3.20}$$

Since $\hat{t}(r) = t_0 - r$ when we choose $R' = 1$ on the null cone, $\dot{R}'(\hat{t},r)$ is given by

$$\dot{R}'(\hat{t},r) = \frac{1}{3}\left[\frac{4M}{3\tau}\right]^{1/3}\left[\frac{M'}{M} - \frac{1+\tau'}{\tau}\right]. \tag{3.21}$$

After some manipulation of the above expression substituted into (3.19), we find that

$$\ln(1+z) = \left(\frac{4M}{3\tau}\right)^{1/3} - \frac{1}{3}\int_0^{r_{em}}\left(\frac{4M}{3\tau^4}\right)^{1/3}dr\,. \tag{3.22}$$

Using (3.14) and (3.15) this equation may be written as

$$\ln(1+z) = \left(1 - \frac{d\hat{R}}{dr}\right) - \frac{1}{2}\int_0^{r_{em}}\left(1 - \frac{d\hat{R}}{dr}\right)^2 / \hat{R}\,dr \tag{3.23}$$

so we can now determine the redshift-area distance relation.

[9]The standard formula $1+z = (u^a k_a)_{em}/(u^a k_a)_{ob}$ is not useful in this gauge since $k^a = (R', -1, 0, 0) = (1, -1, 0, 0)$ is not an affinely parametrized geodesic, though it is tangent to the past null cone.

3.2.1.2 The Friedmann-Lemaître Limit

The characterisation of the FL limit for parabolic LTB models is that the bang time surface is simultaneous. So $t_B(r) = t_{B\mathrm{FL}} = \text{constant}$; from whence

$$R_{\mathrm{FL}}(t,r) = \left[\frac{9}{2}M_{\mathrm{FL}}(r)(t - t_{B\mathrm{FL}})^2\right]^{1/3}, \quad R'_{\mathrm{FL}}(t,r) = \frac{3}{2R_{\mathrm{FL}}^2}M'_{\mathrm{FL}}(r)\,(t - t_{B\mathrm{FL}})^2\,. \tag{3.24}$$

The freedom left here in $M_{\mathrm{FL}}(r)$ is just essentially the coordinate freedom, corresponding to the freedom of choice of r. The above relations determine the FL density

$$\rho_{\mathrm{FL}}(t) = \frac{1}{6\pi(t - t_{B\mathrm{FL}})^2} \tag{3.25}$$

which is spatially homogeneous as required, unaffected by $M_{\mathrm{FL}}(r)$. It is usual to set $t_{B\mathrm{FL}} = 0$.

As we would eventually like to compare our LTB model as chosen above to an underlying FL model, it is appropriate to write the FL limit in the same kind of coordinate system. Consider light rays coming in to the event $(t = t_1, r = 0)$ in a FL model. When we choose coordinates for which $R'_{\mathrm{FL}}(t,r) = 1$ on the null cone, the past null cone can be located by $\hat{t} = t_1 - r - t_{B\mathrm{FL}} = t_1 - r$. (We use t_1 rather than t_0 here, as we will need to distinguish LTB and FL values later on.) As a limit of the flat LTB model in these coordinates, the FL form of $M(r)$ is obtained from setting $\tau = t_1 - r$ in (3.9). This yields

$$M_{\mathrm{FL}} = 6\left[t_1^{1/3} - (t_1 - r)^{1/3}\right]^3 \qquad (M_{\mathrm{FL}}(0) = 0) \tag{3.26}$$

$$\hat{R}_{\mathrm{FL}} = 3\left[t_1^{1/3} - (t_1 - r)^{1/3}\right](t_1 - r)^{2/3} \qquad (R_{\mathrm{FL}}(0) = 0)\,. \tag{3.27}$$

We note that this (3.26) in conjuction with (3.24) implies that

$$R_{\mathrm{FL}}(t,r) = 3\left[t_1^{1/3} - (t_1 - r)^{1/3}\right]t^{2/3} \quad , \quad R'_{\mathrm{FL}} = \frac{3M'_{\mathrm{FL}}}{2R_{\mathrm{FL}}^2}t^2 = \frac{t^{2/3}}{(t_1 - r)^{2/3}}\,. \tag{3.28}$$

The RW metric that results is, from (3.28) and (3.1),

$$ds^2 = -dt^2 + t^{4/3}\left\{\frac{1}{(t_1 - r)^{4/3}}dr^2 + 9\left[t_1^{1/3} - (t_1 - r)^{1/3}\right]^2 d\Omega^2\right\}\,. \tag{3.29}$$

These coordinates are singular at the particle horizon, $r = t_1$ (when the past null cone of $t = t_1$ runs into the initial singularity). Thus they are valid for $0 \leq r < t_1$. The FL redshift-distance formula can be obtained by inserting the FL forms of $M(r)$ and $\tau(r)$ into equation (3.22). That is

$$z(r) = \left(\frac{t_1}{t_1 - r}\right)^{2/3} - 1 \qquad \Longleftrightarrow \qquad r(z) = t_1 \left[\frac{(1+z)^{3/2} - 1}{(1+z)^{3/2}}\right] . \tag{3.30}$$

3.2.1.3 Averaging and Fitting

We want to compare and contrast total areas of wavefronts at given redshifts of an inhomogeneous model to those of the corresponding FL model of density equal to the inhomogeneous density perfectly smoothed. This must be done with respect to the inhomogeneous metric because physically the smoothing does not occur.

Perhaps the crucial part of our analysis is that we ensure that we compare with the FL model with the correct average density. We define the *average* or *background* FL model to be the one that matches on at the particle horizon where $\tau = 0$, $r = r_\Sigma$, using the Darmois-Israel boundary conditions [12, 35]. We match the first and second fundamental forms – the intrinsic metric and extrinsic curvature – of this timelike (comoving) boundary surface Σ, which amounts to specifying that the metric and its first derivative in the adjacent spacetimes remain continuous over the matching surface. In our case,

$$R_{\text{LTB}}|_\Sigma = R_{\text{FL}}|_\Sigma \tag{3.31}$$

and the background model must be parabolic if the inhomogeneous one is; or vice versa.

The matching must hold over all of Σ; that is, at all times – so

$$\dot{R}_{\text{LTB}}\big|_\Sigma = \dot{R}_{\text{FL}}\big|_\Sigma \tag{3.32}$$

and thus, by (3.2),

$$M_{\text{LTB}}|_\Sigma = M_{\text{FL}}|_\Sigma \, . \tag{3.33}$$

Thus it is sufficient to match the masses at Σ, and synchronise the starting times (bang times) when $R_{\rm LTB}|_\Sigma = 0 = R_{\rm FL}|_\Sigma$. In general, we do not expect the FL radial coordinate on Σ ($r_{\rm FL}|_\Sigma$) to be the same as the LTB one there ($r_{\rm LTB}|_\Sigma = r_\Sigma$) since the coordinate condition $\hat{R}' = 1$ holds on the null cone, whose locus is model dependent.

For a parabolic LTB model with metric (3.1) and density given by (3.5), the background density $\rho_{\rm FL}$ is the same as that obtained by integrating over constant time slices. $\langle\rho\rangle = \dfrac{\overline{M}}{\text{volume}}$ where $\overline{M}(r)$ as defined by equation (2.18) in the parabolic case is just $M(r)$.

$$\begin{aligned}
\langle\rho\rangle_{t_0,r_\Sigma} &= \left(\int_0^{2\pi}\int_0^{\pi}\int_0^{r_\Sigma} \rho\sqrt{^3g}\, dr d\theta d\phi\right) / \left(\int_0^{2\pi}\int_0^{\pi}\int_0^{r_\Sigma} \sqrt{^3g}\, dr d\theta d\phi\right) \\
&= \left(\int_0^{r_\Sigma} \frac{M'}{R^2R'}\sqrt{R'^2R^4}dr\right) / \left(4\pi\int_0^{r_\Sigma}\sqrt{R'^2R^4}dr\right) \\
&= \frac{3}{4\pi}\frac{M(r_\Sigma)}{[R(r_\Sigma,t_0)]^3} \\
&= \frac{1}{6\pi(t_0 - t_B(r_\Sigma))^2} = \rho_{\rm FL}
\end{aligned} \tag{3.34}$$

where equation (3.3) was used.

One important point that must be made here is that a covariant averaging procedure does not exist as yet. We have used here an averaging method which is 'natural' for the comoving synchronous coordinates which lead to a $3+1$ foliation of spacetime. However, the same model in different (for example observational) coordinates would suggest a different averaging procedure which could conceivably yield different results. Therefore the claim [72] that the wavefront areas obtained in the inhomogeneous model and the averaged model are the same already seems highly unlikely in that it is not coordinate independent.

3.2.2 Results

We use geometric units such that $G = c = 1$. If we choose a unit of time T_G *seconds* to be 1 geometric time unit (*gtu*), then the geometric units of length, mass, density, etc. are fixed by 1 *glu* $= L_G = cT_G$ *metres*, 1 *gmu* $= M_G = (c^3/G)T_G$ *kg*, 1 *gmu glu*$^{-3}$ $= \rho_G =$

$(1/G)T_G^{-2}$ kg m^{-3}. For the purposes of this work, we want units suitable to cosmological scales, so we specify that one cosmological time unit, 1 ctu, is ten billion years – of the order of the age of the universe. This gives us Table 3.1.

	Time	Length	Mass	Density
Cosmological	1 ctu	1 clu	1 cmu	1 $cmu\ clu^{-3}$
SI	3.156×10^{17} s	9.461×10^{25} m	1.275×10^{53} kg	1.505×10^{-25} kg/m^3
Astronomical	10 Gyr	3.066 Gpc	6.409×10^{22} $M_\odot$	1.505×10^{-28} g/cc

Table 3.1: Correspondence Between Cosmological, SI and Astronomical Units

The first subsection (3.2.2.2) gives a very simple model which satisfies the criteria for a reasonable cosmological model (with the classical Copernican principle dropped) and which provides a *proof that there exist physically reasonable density behaviours which lead to a nonzero magnification or shrinking.* It is obvious that averaging over the sky will not remove this effect since the model is already spherically symmetric. The second model (3.2.2.3) does the same, but is smoother at the origin and displays interesting behaviour in redshift space.

These two models are obtained by choosing the observer area distance function, which is the easiest way of solving this problem.

3.2.2.1 Form of Perturbation and General Results

It is not easy to choose a form of area distance function for the inhomogeneous model which results in reasonable physical behaviour. So instead we choose it in the form of a 'perturbation' from a flat Friedmann model; that is,

$$\hat{R}(r) = \hat{R}^u_{\text{FL}}(r)(1 + \delta(r)) \tag{3.35}$$

where, from (3.27), $\hat{R}^u_{\text{FL}}(r) = 3[{t_u}^{1/3} - (t_u - r)^{1/3}]\,(t_u - r)^{2/3}$ is the area function of an *underlying* FL model of age $t_1 = t_u$. (This 'underlying' FL model is a mathematical device with no physical significance. It can not be considered a background or average model since

we have not restricted $\delta(r)$ to average out to zero in any sense.) In principle, one should choose a density function and then determine the area distance function from it or risk the possibility of assuming the result. However, if we can show that the above choice of $\hat{R}$ leads to a density profile with reasonable physical behaviour, this would suffice – since if we had initially chosen that density function, it would lead to an $\hat{R}$ as chosen above. We will show that this is indeed the case and also indicate that the model is free of shell crossings.

Obviously, for $\delta(r)$ smooth and finite, $\hat{R}(r)$ is zero at the same places as $\hat{R}^u_{\rm FL}(r)$, i.e. at $r = 0$ and at $r = t_u$. For this form of perturbation, in terms of the convenient parametrisation $v = r/t_u$, we find

$$X \equiv \left[\frac{1}{(1-v)^{1/3}} - 1\right] \tag{3.36}$$

$$M = \frac{3}{2} t_u X(1-v)(1+\delta)[2X(1+\delta) - \delta - 3t_u X(1-v)\delta']^2 \tag{3.37}$$

$$\tau = \frac{2t_u X(1-v)(1+\delta)}{[2X(1+\delta) - \delta - 3t_u X(1-v)\delta']} \tag{3.38}$$

$$t_B = t_0 - r - \tau \tag{3.39}$$

$$\begin{aligned} 8\pi\hat{\rho} &= \frac{2X(1+\delta) - \delta - 3t_u X(1-v)\delta'}{9[t_u X(1-v)(1+\delta)]^2}\{2X(3+4\delta)(1+\delta) - \delta(1+\delta) \\ &- 3t_u X(1-v)(5+6\delta)\delta' + 36t_u X^2(1-v)(1+\delta)\delta' \\ &- 9{t_u}^2 X^2(1-v)^2[2(1+\delta)\delta'' + \delta'^2]\} \end{aligned} \tag{3.40}$$

$$\begin{aligned} \frac{d\ln(1+z)}{dz} &= \{4X(1+2\delta)(1+\delta) - \delta^2 - 6t_u X(1-v)(2+3\delta)\delta' \\ &+ 36t_u X^2(1-v)(1+\delta)\delta' - 9{t_u}^2 X^2(1-v)^2[2(1+\delta)\delta'' + \delta'^2]\} \\ &/ \; [6t_u X(1-v)(1+\delta)]\,. \end{aligned} \tag{3.41}$$

If $\delta(0) \neq 0$ we find the unphysical limits $\tau(0) = 0$ and $\hat{\rho}(0) = \infty$. Thus we set $\delta(0) = 0$, obtaining the following limiting values:

$$M(0) = \left.\frac{2(1 - 3t_u\delta'(r))^2 r^3}{9{t_u}^2}\right|_{r\to 0} = 0 \tag{3.42}$$

$$\tau(0) = \frac{t_u}{1 - 3t_u\delta'(0)} \tag{3.43}$$

$$8\pi\hat{\rho}(0) = \frac{4(1-3t_u\delta'(0))^2}{3{t_u}^2} \tag{3.44}$$

$$\left.\frac{d\ln(1+z)}{dr}\right|_{r=0} = \frac{2(1-3t_u\delta'(0))}{3t_u} \tag{3.45}$$

and

$$M(t_u) = 6t_u(1+\delta(t_u))^3 \tag{3.46}$$

$$\tau(t_u) = (t_u - r)|_{r\to t_u} = 0 \tag{3.47}$$

$$8\pi\hat{\rho}(t_u) = \left.\frac{4(3+4\delta(r))}{9(t_u-r)^2}\right|_{r\to t_u} = \infty \tag{3.48}$$

$$\left.\frac{d\ln(1+z)}{dr}\right|_{t_u} = \left.\frac{2(1+2\delta(r))}{3(t_u-r)}\right|_{r\to t_u} = \infty\,. \tag{3.49}$$

(The limits for the background FL model are obtained by setting $\delta = 0 = \delta' = \delta''$ and replacing t_u by t_b.) From numerical experimentation we concluded, in order to avoid shell crossings, that $\delta(r)$ must remain sufficiently far away from zero over most if not the entire range of $r > 0$, and certainly near $r = t_u$. We want the proper time from the bang surface to the null surface on the central worldine to be the 'true' age of the universe; that is, we want it to be t_0, the time at the origin of the LTB model. By setting $\tau(0) = t_0$ in (3.43), the age of the underlying model is determined

$$t_u = t_0\,(1 - 3\,t_1\,\delta'(0))\ . \tag{3.50}$$

The parameter t_u is the r-coordinate value at which the null cone of the LTB model intersects the bang. We will average quantities on this scale; that is to say, we shall take $r_\Sigma = t_u$. We match this inhomogeneous universe to a flat FL model at the surface r_Σ by equating the masses and bang times at that point. This then determines the time $t_1 = t_b$ in the *background* FL model which we will use for our comparison. At $r = t_u$, $\hat{R} = 0$ and (3.46) shows that at this point,

$$M(t_u) = M^u_{\rm FL}(t_u)\,(1+\delta(t_u))^3 = 6t_u\,(1+\delta(t_u))^3\,.$$

In the background FL model the value of the mass at Σ is $6t_b$ and this is what we have to match the inhomogeneous mass to. This gives us a value of the age for the background flat FL model of

$$t_b = t_u\,(1 + \delta(t_u))^3\ . \tag{3.51}$$

3.2.2.2 A Regular Model which Exhibits Shrinking and Magnification

The following simple example is physically well behaved, being free of shell crossings at all times in its evolution for $r \leq t_u$. Since $t'_B \neq 0$ at the origin, the model is not as smooth there as one would like, but there are no physical problems. We choose $\delta(r)$ for our first model, LTB1, to be

$$\delta(r) = -\frac{1}{5}\sin\left(\frac{0.8\pi r}{t_u}\right)\ . \tag{3.52}$$

When we set $\tau(0) = t_0 = 1$ then

$$t_u = t_0\left(1 + \frac{12\pi}{25}\right) \tag{3.53}$$

and the age for the background flat FL model, after matching the masses, is

$$t_b = t_u\left(1 - \frac{\sin 0.8\pi}{5}\right)^3\ . \tag{3.54}$$

The calculation of the redshift was done by a numerical quadrature of (3.23).

It is important to plot these quantities in terms of the observable quantity z for two reasons. First of all, in the transformation $r \to z$, the possibility exists that the area distances of the flat and inhomogeneous models might transform into each other. Secondly, under certain circumstances the redshift becomes disordered with distance and unexpected behaviour might occur, as the next model (3.2.2.3) illustrates.

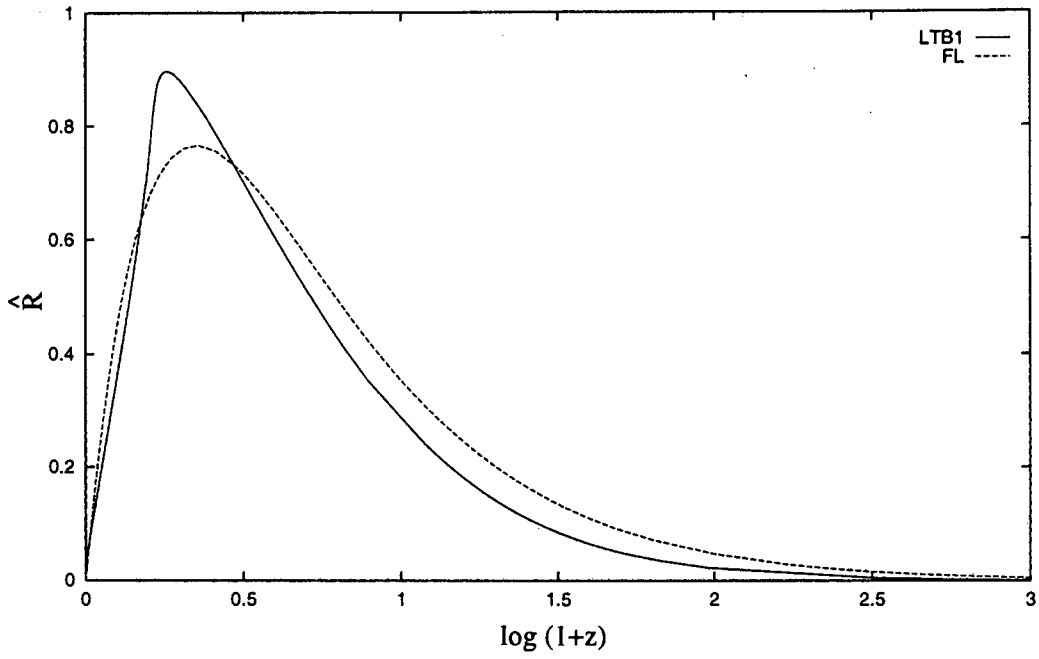

Figure 3.2: A plot of area distance against redshift on the past null cone of the inhomogeneous model LTB1 and the corresponding FL background area. The units of $\hat{R}$ are cosmological length units, and all the figures use base 10 logs. This shows that there are systematic shrinking ($\hat{R} > \hat{R}_{FL}$) and magnification ($\hat{R} < \hat{R}_{FL}$) effects due to purely radial lensing, which obviously cannot be removed by averaging over large angular scales or even the whole sky. Effects of true lensing in a more realistic universe would be imposed on top of this.

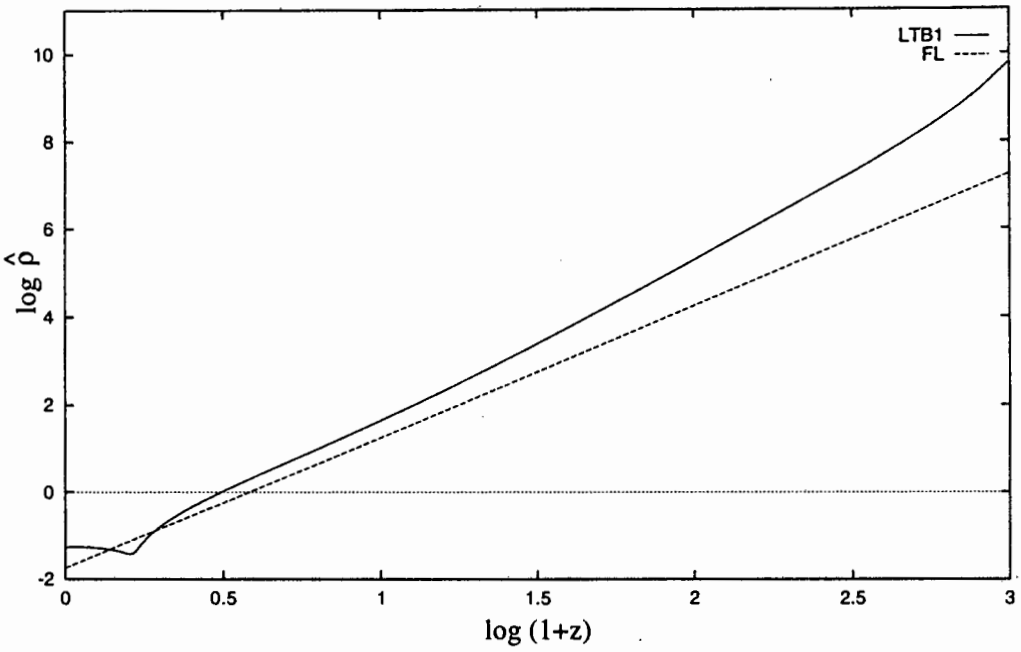

Figure 3.3: The density of matter on the *past null cone* (that is, what would actually be observed) in the models of Figure 3.2, LTB1 and its corresponding background FL model. The units are cosmological density units ($cmu\ clu^{-3}$). When comparing with Figure 3.2, we see that roughly speaking, magnification occurs for objects in or just beyond an overdense region, and shrinking occurs for objects in or just beyond an underdensity.

3.2.2.3 A Regular Model with Multivalued Observations

As an illustration of how different the physical quantities plotted against radial coordinate r as opposed to those same quantities plotted against redshift z may appear, we present here an LTB model for which the redshift becomes disordered with distance at some points and then ordered again at later points.

The universe is chosen as above but with a 'perturbation function' of

$$\delta(r) = -\frac{1}{4}\sin\left(\frac{0.75\pi r}{t_u}\right) - \frac{1}{4^6}\left(\frac{11}{\pi} + \frac{3}{2}\right)\left[1 - \cos\left(\frac{4\pi r}{t_u}\right)\right]. \tag{3.55}$$

This model, which we call LTB2, is also free of shell crossings at any time for $r \leq t_u$ and has a completely smooth and regular origin (where $t'_B = 0$). Setting $\tau(0) = t_0 = 1$ once again gives

$$t_u = t_0\left(1 + \frac{9\pi}{16}\right) \tag{3.56}$$

and

$$t_b = t_u\left(1 - \frac{\sin 0.75\pi}{4}\right)^3. \tag{3.57}$$

which are different from those of LTB1.

This model provides a good illustration of why one has to be careful in ascribing physical behaviour in a certain coordinate system. Viewed as functions of r, $\hat{R}$ and $\hat{\rho}$ have fairly standard behaviour, but viewed in terms of the observable quantity z, the density and area distance become multivalued. Hence, three objects with the same intrinsic luminosity located at different distances appear at the same z, with three different apparent luminosities (or area distances).

Our numerical experiments indicate that the redshift on the light cone is most sensitive to perturbations in the vicinity of the maximum in $\hat{R}(z)$. All our models in which $dz\,/\,dr$ became negative did so in this region. The looping behaviour in the $\hat{R}$ vs $\log(1+z)$ plot

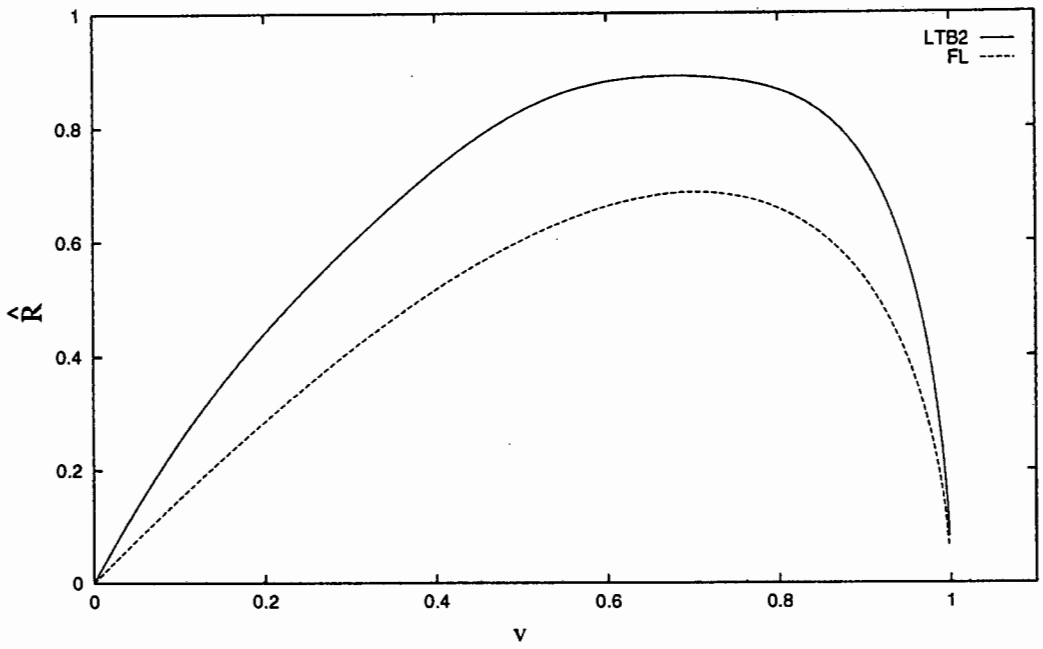

Figure 3.4: The LTB area distance function $\hat{R}(r)$ on the past null cone and its background FL analogue ($\hat{R}_{FL}$) for the second LTB model, LTB2, given in cosmological units. The horizontal variable is $v = r/t_u$ or r/t_b for LTB2 and FL respectively. The physical behaviour of LTB2 as plotted against v appears normal.

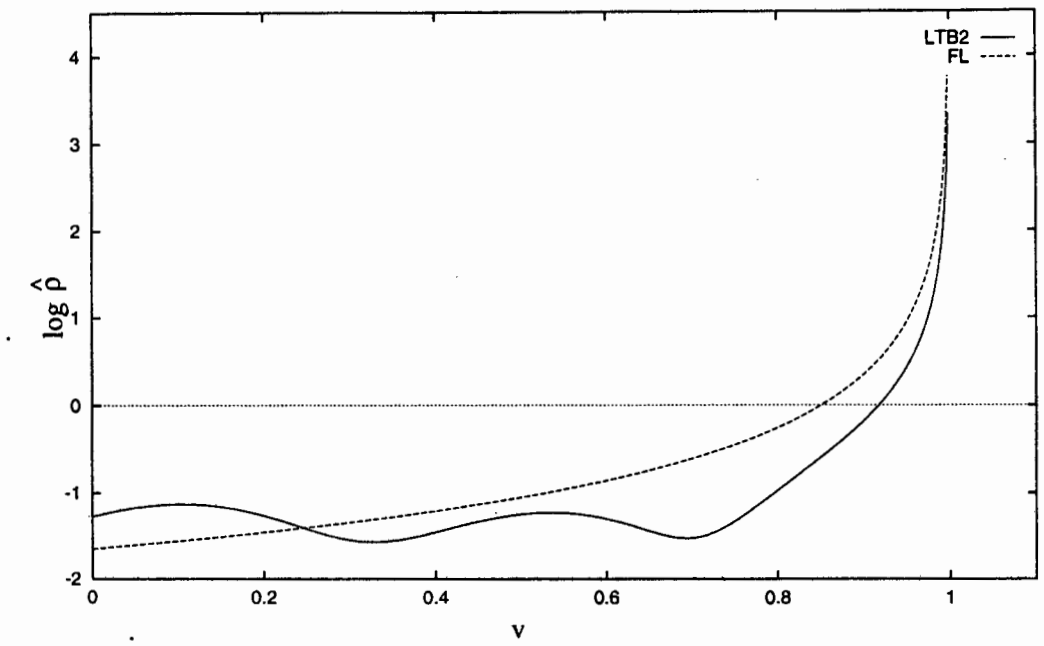

Figure 3.5: The densities for the second LTB model and its background FL model ($\hat{\rho}$ and $\hat{\rho}_{FL}$, in cosmological units) on the past null cone. Again, LTB2's inhomogeneous profile vs v appears quite acceptable.

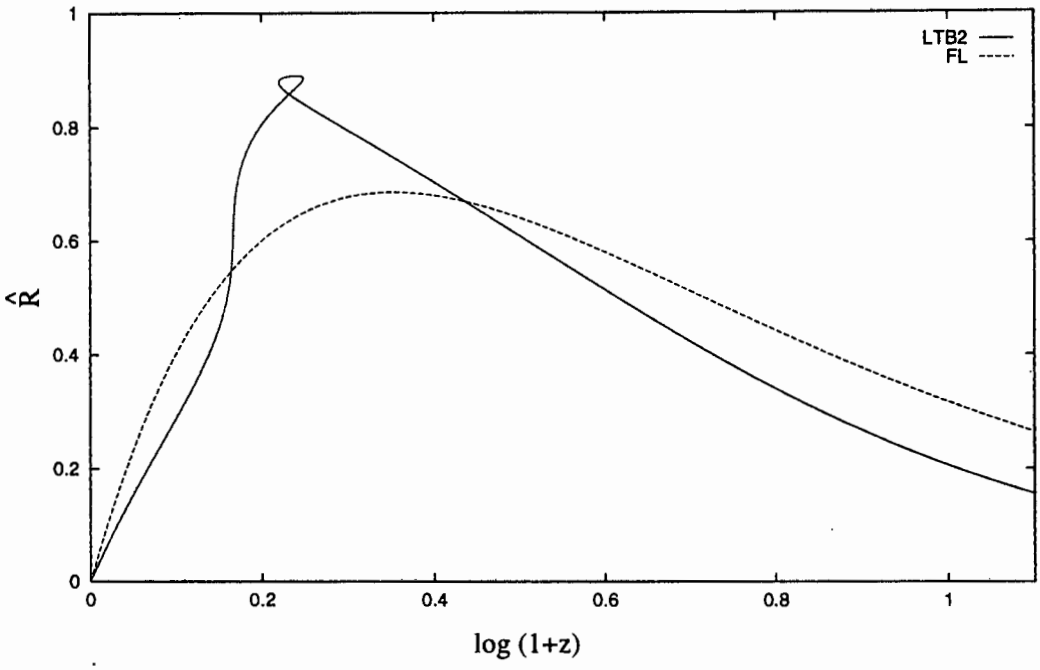

Figure 3.6: A plot of area distance against redshift for model LTB2 and the background FL model. The interesting point to note is that at some redshifts the area distance in the LTB model is multivalued. For $\log_{10}(1+z) \geq 1$ the graph looks very much like Figure 3.2.

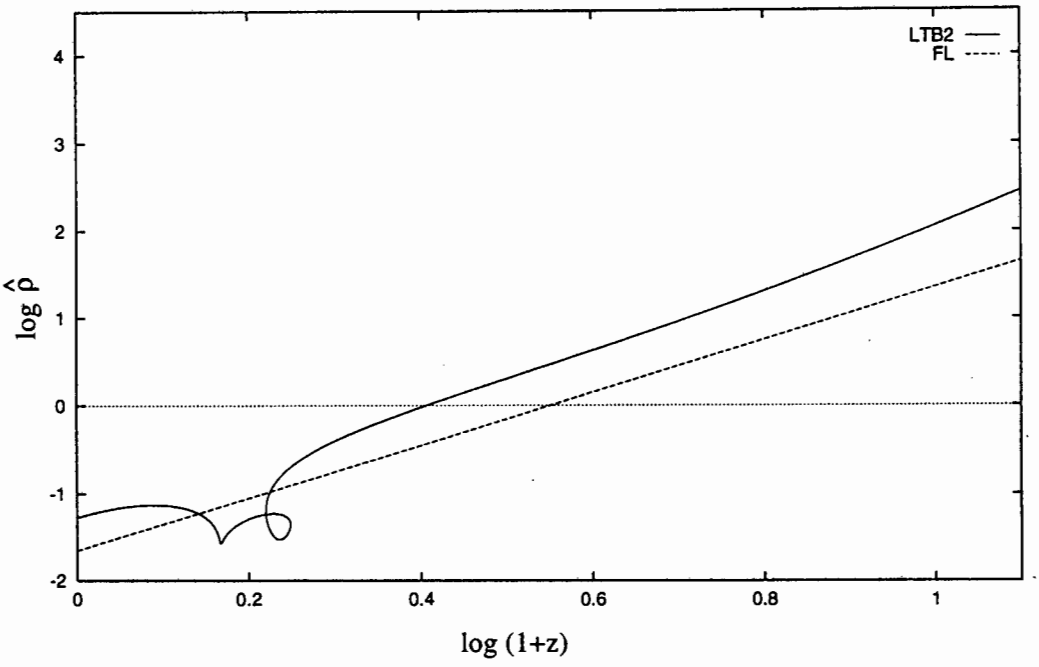

Figure 3.7: The densities ($\hat{\rho}$ and $\hat{\rho}_{FL}$) on the past null cones vs z for model LTB2 and its background FL model. Note the quaint 'looping' behaviour. For $\log_{10}(1+z) \geq 1$ the graph looks very much like Figure 3.3.

occurs when the maximum and minimum in the $\log(1+z)$ vs r graph bracket the maximum in the $\hat{R}$ vs r graph. Similarly, perturbations more easily generate a maximum and minimum in the $\hat{\rho}(z)$ near the maximum in $\hat{R}$, hence the loop in that graph.

3.2.3 Conclusions

The general belief that photon conservation implies that the total area of an incoming wavefront must be the same as in the background, matter-averaged, FL model has been disproved in this chapter. The spherically symmetric model used here is simple but effective, since averaging over direction cannot change the results. In more realistic models of the lumpy universe this effect will still be present, and we expect full gravitational lensing to occur, resulting in more significant deviations from the FL formula.

This investigation used a parabolic LTB model, where the areal radius $\hat{R}$ is also the area distance of the 2-sphere wavefronts of the past null cone. The density in the LTB model is averaged to give a background Einstein-de Sitter ($\Omega = 1$) model, and it is tested against this model. Although there exists no covariant way to perform this averaging, we use the 'natural' one defined by the use of junction conditions, here equivalent to the one used in astrophysical problems: that is, averaging on constant time slices. Some may argue that the 'natural' way of averaging for this kind of study, which involves observations, is to average the density on the null cone, but this procedure appears rather mysterious. It certainly is not easy to define, mainly for the reason that, as the averaging domain on the null cone is increased, the density in general will increase because we are looking back into the past and would thus have to account for evolution of sources.

The results show that it is quite easy to have areas in the inhomogeneous models which differ significantly from areas in the background, matter-averaged FL model. The result may either be shrinking (the background FL area distance underestimates the real area distance at that redshift) or magnification (background FL area distance is an overestimate). The

presence of loops in the $\hat{R}$-z and $\hat{\rho}$-z graphs is analogous to the well known 'finger of God' effect familiar in redshift maps of the galaxy distribution (see Figure 4.1).

The choice of radial coordinate employed here (which locates the observer's null cone) will be of use in future analyses of observations in these isotropic dust models.

An important caveat is that since the LTB model does not allow for formation of caustics in the null cone of the central observer, it cannot be considered a useful model for obtaining quantitative 'real world' results. Rather this contribution should be viewed as a proof that even purely radial lensing distorts the area distance-redshift relation significantly. If the observer moves away from the central position, then continuity ensures that the radial effects found here will still be present, and the effects of true lensing will be superimposed. As argued in [20, 64], we expect caustics to skew the area towards larger values, so that most objects in the universe are demagnified.

The importance of all this is that it opens up the way for considering the effects of lensing by inhomogeneities on large angular-scale number counts and CMB observations (for example, COBE), as opposed to limiting discussion to lensing effects on small scales.

Chapter 4

Clumps Evolving to Voids

The fleet astronomer can bore
And thread the spheres with his quick-piercing mind:
He views their stations, walks from door to door,
Surveys, as if he had designed
To make a purchase there; he sees their dances,
And knoweth long before
Both their full-eyed aspécts, and secret glances.

– George Herbert

In the inflationary universe paradigm, it is believed that the observed universe is very nearly flat (that is the density parameter – the sum of all contributions – is close to 1). The density of baryons – which can be obtained from primordial nucleosynthesis theory – is however very small and this requires that most matter is non-baryonic (so called 'dark matter'). The traditional view of structure formation is that baryonic matter fell into the high density peaks of dark matter and became luminous forming stars and galaxies. The stationary view, in which matter remains essentially fixed in comoving coordinates[1], may well be a good approximation if the initial density field is simply amplified by gravitational

[1]In geometrical terms, the stationary approximation is governed by a mapping which preserves extremal points of the density field.

processing, but when the matter content of the pre- and post-decoupling epochs is viewed from a hydrodynamical point of view as a fluid in high-temperature plasma or quasi-plasma state, one would expect shock waves and other spatial gradients to exist (even if their amplitudes were small). This is exemplified by the discovery of nonlinear and solitonic waves in molecular clouds [1]. Indeed, large scale inhomogeneities and flows have been shown to be a pervasive influence on the behaviour of the universe on scales of (at least) up to 100 Mpc. (Cf. for example [54]).

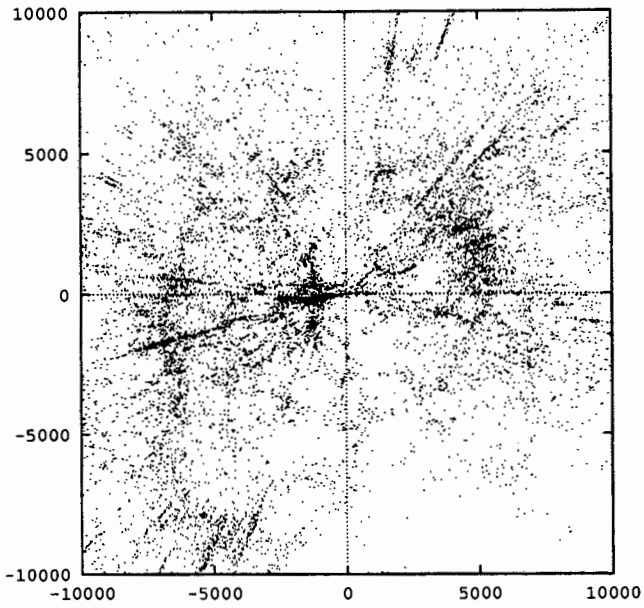

Figure 4.1: A projection onto the plane of a 3000 km/s thick slice of Tony Fairall's compilation of all published redshifts for galaxies in the Southern hemisphere added to the redshifts from ZCAT compiled by John Huchra for the Northern hemisphere. No selection criteria have been taken into account. The axes are in km/s. The apparent radial alignment some of these galaxies exhibit are the well known 'fingers of God' effect. They are due to the fact that galaxies within bound clusters exhibit a large range of peculiar motions which is not taken into account by surveyors, as it is assumed all shifts are due to motions directly from or towards us. (Courtesy Paul Haines.)

The now undisputed existence of large-scale (Dekel (1994) [14]) cosmic flows lends more credence to the idea that perhaps the stationary approximation, used ubiquitously in structure formation, is not as good as assumed. Large flows (on the scale of 15000 kms^{-1}) have been reported by various authors [58]. The existence of such large, relatively high-amplitude cosmic flows today implies that one of the assumptions going into almost all the standard structure formation theories may be dubious to some degree. The bulk flow reading of $700 \pm 170 kms^{-1}$ found for all Abell clusters with redshifts less than $15000 kms^{-1}$ strongly excludes any of the popular models with Gaussian (that is to say cold) initial condiditions, although these investigations have been done in flat (Einstein de Sitter) space[2].

In this context, the LTB universe is interesting as one may analytically study the evolution of spherically symmetric inhomogeneities. The discovery of large scale voids and walls (honeycombs) in the late 70's and early 80's sparked interest in the LTB model as a means of investigating these, and other similar, structures (for example [51, 52, 33, 59, 48, 60, 40, 56]). Many of these studies considered universes composed of LTB overdense and/or underdense regions matched onto RW exteriors – so-called Swiss Cheese models.

The nonlinear effects of large scale clumps (for example [57]) and voids ([2, 60]) on the production of anisotropies in the CMB has been studied using LTB models numerically. The results have been that a large part of the temperature anisotropies in the background radiation (the dipole component) may be completely due to large scale structures, but leave open the origin of other sources (for example quadrupole) as truly cosmological.

These studies concentrated on the description and feasibility of spherical inhomogeneities, and were not too concerned with determining under what conditions structures could change radically with evolution. In this piece of work we will attempt to do just that.

At the centre of symmetry of an LTB universe, we must generically have a position of

[2]One would expect these results to be altered in open spatial sections on large scales.

extreme density – that is either a maximum or a minimum. Thus at the centre it is not feasible to study the question of density waves, per se, since a wave is defined by the fact that a maximum (or minimum) moves at some velocity away from the worldline. But it is, in principle, possible to study density waves analytically away from the centre and in particular at the centre we can ask the question: '*under what conditions will a density maximum evolve into a density minimum or vice versa?*'. This is a first step towards a study of cosmic flows in this model, since if this question can be answered in the affirmative, then it would naturally follow that in some region around the centre over the time elapsed a maximum (or minimum) has to be travelling away from the centre.

This would raise questions about the validity of the standard model of structure formation. It is particularly important to analyses of the most succesful cosmic experiment to date, namely COBE, where the data (for example, hot spots and cold spots) on the last scattering surface is 'transferred' to the current epoch by use of a function which does not assume that the peaks in the matter distribution may change to troughs.

4.1 Preliminaries and Programme

We are interested in whether the profile of a density inhomogeneity can change significantly with evolution. Specifically, we want to know whether a central maximum in density can evolve into a central minimum, or vice versa. We call this phenomenon Density Profile Inversion (DPI). For our investigation we use the simplest inhomogeneous cosmological solution to the Einstein field equations, the LTB model.

The expression for the energy density, $\rho = \rho(t, r)$, in the model is well-known (equation (2.10)). We have

$$8\pi\rho = \frac{2\,M'}{R^2\,R'}.$$

We define a 'scale radius', $p(r)$, and 'scale time', $q(r)$, for non-parabolic models as follows:

$$p(r) = \frac{M}{\pm E} \tag{4.1}$$

and

$$q(r) = \frac{M}{\sqrt{\pm 2E^3}} \tag{4.2}$$

whilst for parabolic models there are no natural scale lengths or times, but we can use

$$p = 2M = q\,.$$

The '+' is applicable in hyperbolic models and the '$-$' is used for elliptic models. In a recollapsing model, the point of maximum expansion is given by $p(r)$ and the time from big bang to big crunch is $\pi\, q(r)$. From the definition of $p(r)$ and $q(r)$ we can write equation (2.12) to equation (2.14) as

$$R = \frac{p}{2}\phi_0, \qquad \xi = \frac{2\,(t - t_B)}{q} \tag{4.3}$$

where

$$\phi_0 = \begin{cases} \cosh(\eta) - 1, \\ (1/2)\eta^2, \\ 1 - \cos(\eta), \end{cases} \qquad \xi = \begin{cases} \sinh(\eta) - \eta, & E > 0 \\ (1/6)\eta^3, & E = 0 \\ \eta - \sin(\eta), & E < 0 \end{cases} \tag{4.4}$$

4.1.1 Procedure

Much of the calculational work in the following sections involve considerable, albeit straightforward, computations. In many cases, especially the final results, the computer algebra package *Maple V (various versions)* was used to check individual results.

The fractional spatial gradient of the density is obtained by differentiating the density with respect to R on a constant t-slice. Since R is a physically invariant quantity – the areal radius – this will give us results which are not coordinate dependent.

We allow coordinate radius r to be a function of t and R, that is $r = r(t, R)$. For $R = R(t, r)$ we have

$$dR = \left.\frac{\partial R}{\partial t}\right|_r dt + \left.\frac{\partial R}{\partial r}\right|_t dr$$

and for $r = r(t, R)$

$$dr = \left.\frac{\partial r}{\partial t}\right|_R dt + \left.\frac{\partial r}{\partial R}\right|_t dR$$

Now on a *constant time surface*, $dR = \left.\frac{\partial R}{\partial r}\right|_t dr$ and $dr = \left.\frac{\partial r}{\partial R}\right|_t dR$. Therefore,

$$\left.\frac{\partial r}{\partial R}\right|_t = 1/\left.\left(\frac{\partial R}{\partial r}\right)\right|_t = \frac{1}{R'}.$$

We can take a slice in time in the natural way since the coordinate time t is also proper time for comoving dust in a synchronous metric and so also physically invariant.

Now for any function of r, say $F(r) = F(r(R, t))$ we define

$$\left.\frac{\partial F}{\partial R}\right|_t \equiv \partial_R F = \frac{dF}{dr}\left.\frac{\partial r}{\partial R}\right|_t = \frac{F'}{R'}$$

So the energy density on a hypersurface of constant time, equation (2.10), can be written as

$$8\pi\rho = \frac{2\,\partial_R M}{R^2} \tag{4.5}$$

From the above equation we find the fractional spatial gradient of the density to be

$$\frac{\partial_R \rho}{\rho} = \frac{\partial_{RR} M}{\partial_R M} - \frac{2}{R} \tag{4.6}$$

where we have determined

$$\partial_{RR} M \equiv \left.\frac{\partial^2 M}{\partial R^2}\right|_t = (M'' - (\partial_R M)R'')/(R')^2 \tag{4.7}$$

Our method for this investigation is straightforward. We require that the density be smooth through the origin of our coordinate system. Thus the spatial gradient of the density

has to vanish at $R(t, r = 0)$ for all t. This would then impose certain restrictions on the three arbitrary functions $M(r)$, $E(r)$ and $t_B(r)$ and their derivatives for this density profile to hold. The change in concavity of the density profile at the origin is determined by the sign of the second radial derivative of the density at that point.

4.1.2 The Hyperbolic Case

We continue our investigation in the forever expanding model. There are three reasons why we do this. One is because recent analysis of current observations provide a strong case for an Ω that is less than unity (Cf. section 2.3.1). The other reason is more of a practical, intuitive nature. In an elliptic model, if we consider an initially overdense spherically symmetric shell, the conditions under which this will change to a void would be predictably stringent, because we know that each shell of matter must eventually recollapse. This may put bounds on how low the density can be in a particular region of space at any time. In fact, it has been found that [7] the average density of a void (in an LTB model with simultaneous bangtime) relative to an elliptic background has a lower bound of $8 \times 10^{-30} g/cm^3$; very close to the average cosmic density of $10^{-29} g/cm^3$. Whilst this restriction on the amplitude of the density can be relaxed by a suitable choice of t_B [3], it seems more logical to continue our studies in the hyperbolic model. The final (and undoubtedly the most cogent) reason why we do this is because we haven't gotten round to doing the other case yet. Investigations into the *parabolic* case would be uninteresting because we expect every parabolic model to evolve asymptotically towards Minkowski space at late times.

4.1.2.1 The Spatial Derivatives of Areal Radius

For the required density profile we need expressions for the spatial gradient R' and second and third radial derivatives R'' and R'''. Our task is somewhat complicated by the way R is

[3] Also the boundary of the void was forced to be comoving – shown to be an unstable situation later (Cf. Sato 1984).

defined in the hyperbolic (equation (2.12)) or elliptic (equation (2.14)) cases.

For the purposes of this investigation, we require the expressions for R', R'' and R''' to be in the same form as that for areal radius, R, above; that is we want them explicitly as a sum of a product of functions of r and functions of η. This can be accomplished by a suitable application of the Leibniz rule for differentiation.

We find

$$\frac{\partial R}{\partial r} = \frac{p}{2} u\phi_0 + \frac{p}{2}\frac{d\phi_0}{d\eta} 1/\left(\frac{d\xi}{d\eta}\right)\frac{\partial \xi}{\partial r}$$

where $u(r)$ has been defined as

$$u \equiv (\ln p)' = \frac{M'}{M} - \frac{E'}{E}. \tag{4.8}$$

After some manipulation we obtain

$$\frac{\partial R}{\partial r} = \frac{p}{2} v\phi_2 - \frac{p}{q} t_B{}'\phi_1 + \frac{p}{2} u\phi_0 \tag{4.9}$$

where $v(r)$ is defined by

$$v \equiv \left(\ln \frac{1}{q}\right)' = \frac{3E'}{2E} - \frac{M'}{M}. \tag{4.10}$$

We proceed in a similar fashion to obtain an expression for the second radial derivative:

$$\begin{aligned} \frac{\partial^2 R}{\partial r^2} &= \frac{p}{2} v^2\phi_5 - \frac{p}{q} t_B{}' v\phi_4 + \frac{2p(t_B{}')^2}{q^2}\phi_3 + \frac{p}{2}(v' + 2uv)\phi_2 \\ &- \frac{p}{q} t_B{}'(w+u)\phi_1 + \frac{p}{2}(u' + u^2)\phi_0 \end{aligned} \tag{4.11}$$

where

$$w(r) \equiv \left(\ln \frac{p}{q} t_B{}'\right)' = \frac{E'}{2E} + \frac{t_B{}''}{t_B{}'}. \tag{4.12}$$

We will also be using the third derivative which can be found by differentiating (4.11).

$$\frac{\partial^3 R}{\partial r^3} = \frac{p}{2} v^3\phi_9 - \frac{p}{q} t_B{}' v^2\phi_8 + \frac{2p(t_B{}')^2}{q^2} v\phi_7 - 4p\left(\frac{t_B{}'}{q}\right)^3 \phi_6$$

$$
\begin{aligned}
&+ \frac{3}{2}\,pv\,(uv+v')\phi_5 - \frac{3p}{2q}\,t_B{}'\,(v'+uv+wv)\phi_4 \\
&+ \frac{6\,p\,(t_B{}')^2}{q^2}\,w\,\phi_3 + \frac{p}{2}(3u^2v+3uv'+3u'v+v'')\phi_2 \\
&- \frac{p}{2q}\,t_B{}'\,(v'+2w'+4u'+2w^2+2uw+2u^2+uv-wv)\phi_1 \\
&+ \frac{p}{2}(u^3+3uu'+u'')\phi_0\,. \qquad (4.13)
\end{aligned}
$$

The ϕ_i are all functions of η and they are listed below:

$$\phi_1(\eta) = \frac{\sinh\eta}{\phi_0} \qquad (4.14)$$

$$\phi_2(\eta) = \sinh\eta\,\frac{\xi}{\phi_0} \qquad (4.15)$$

$$\phi_3(\eta) = -\left(\frac{1}{\phi_0}\right)^2 \qquad (4.16)$$

$$\phi_4(\eta) = \phi_1 - 2\frac{\xi}{\phi_0^2} \qquad (4.17)$$

$$\phi_5(\eta) = \phi_2 - \frac{\xi^2}{\phi_0^2} \qquad (4.18)$$

$$\phi_6(\eta) = 2\frac{\sinh\eta}{{\phi_0}^4} \qquad (4.19)$$

$$\phi_7(\eta) = 3\phi_3 + 6\sinh\eta\,\frac{\xi}{{\phi_0}^4} \qquad (4.20)$$

$$\phi_8(\eta) = \phi_1 - \frac{6\xi}{{\phi_0}^2} + 6\sinh\eta\,\frac{\xi^2}{{\phi_0}^4} \qquad (4.21)$$

$$\phi_9(\eta) = \phi_5 + 2\sinh\eta\,\frac{\xi^3}{{\phi_0}^4} - \frac{2\xi^2}{{\phi_0}^2} = \phi_2 - \frac{3\xi^2}{{\phi_0}^2} + 2\sinh\eta\,\frac{\xi^3}{{\phi_0}^4} \qquad (4.22)$$

with ϕ_0 and ξ given by (4.4). The above functions have a very similar form in the elliptic case.

The above derivatives of R will be used later in our investigations. They have been expressed in terms of u, v and w because if written in terms of M, E and t_B the expressions become a bit messy and are not very useful in that form at this stage. Quantities determined later will be expressed in terms of the latter variables when appropriate.

4.1.2.2 The Smooth Central Density Criteria

We return our attention to equation (4.6); that is,

$$\frac{\partial_R \rho}{\rho} = \frac{\partial_{RR} M}{\partial_R M} - \frac{2}{R}.$$

We require the density to be finite and its gradient to vanish at the origin. Thus, for the required density profile we must have

$$\left.\frac{\partial_R \rho}{\rho}\right|_{r=0} = -\frac{1}{(R')^2}\left[2\frac{(R')^2}{R} + R'' - \frac{M''}{M'}R'\right]\Bigg|_{r=0} = 0 \tag{4.23}$$

(holding in all three geometries). We will refer to equation (4.23) as the 'extremum density criterion'.

Now that we have obtained usable expressions for R' and R'', we can substitute them into equation (4.23) to obtain restrictions on the arbitrary functions $E(r)$, $M(r)$ and $t_B(r)$ for the extreme density criterion to hold.

We find that

$$\frac{1}{(R')^2}\left[\frac{p}{2}v^2(\phi_5 + 2\frac{{\phi_2}^2}{\phi_0}) - \frac{p\,t'_B}{q}v\,(\phi_4 + 4\frac{\phi_1\phi_2}{\phi_0}) + \frac{2\,p\,(t'_B)^2}{q^2}(\phi_3 + 2\frac{{\phi_1}^2}{\phi_0}) - \right.$$
$$\left.\frac{p}{2}(\frac{M''}{M'}v - 6uv - v')\phi_2 - \frac{p\,t'_B}{q}(w + 5u - \frac{M''}{M'})\phi_1 - \frac{p}{2}(\frac{M''}{M'}u - 3u^2 - u')\phi_0\right] \tag{4.24}$$

must vanish at the origin.

We want the density at the origin to be flat at all times. Since the functions of parameter time η are linearly independent of each other, it follows that each of the terms in equation (4.24) must vanish separately if we want the lefthand-side to vanish.

This leaves us with the following conditions which must hold at the origin for the required density profile:

From the first term we get

$$\frac{1}{(R')^2}\left(\frac{M}{E}\right)\left(\frac{3E'}{2E} - \frac{M'}{M}\right)^2\Bigg|_{r=0} = 0 \tag{4.25}$$

whilst the second term gives

$$\frac{1}{(R')^2}(2E)^{1/2}t_B{}'\left(\frac{3E'}{2E}-\frac{M'}{M}\right)\Bigg|_{r=0}=0$$

and the third

$$\frac{1}{(R')^2}\frac{(2E)^2}{M}t_B{}'^2\Bigg|_{r=0}=0\,. \tag{4.26}$$

Note that the second condition is satisfied if the first and third ones are. The fourth term expands to

$$\frac{1}{(R')^2}\left(\frac{M}{2E}\right)\left[\frac{3E'M''}{2EM'}+5\left(\frac{M'}{M}\right)^2+\frac{21}{2}\left(\frac{E'}{E}\right)^2-15\frac{E'M'}{EM}-\frac{3E''}{2E}\right]\Bigg|_{r=0}=0\,.$$

We can combine equation (4.25) with the above (that is subtract $5\times$ equation (4.25)) to get

$$\frac{1}{(R')^2}\left(\frac{M}{2E}\right)\left[\frac{E'M''}{EM'}-\frac{1}{2}\left(\frac{E'}{E}\right)^2-\frac{E''}{E}\right]\Bigg|_{r=0}=0\,. \tag{4.27}$$

The fifth term in equation (4.24) yields

$$\frac{1}{(R')^2}(2E)^{1/2}t_B{}'\left[\frac{M''}{M'}-5\frac{M'}{M}+\frac{9E'}{2E}-\frac{t_B{}''}{t_B{}'}\right]\Bigg|_{r=0}=0\,.$$

We subtract $3\times$ (the coefficient of $\phi_4+4\dfrac{\phi_1\phi_2}{\phi_0}$) to obtain

$$\frac{1}{(R')^2}(2E)^{1/2}t_B{}'\left[\frac{M''}{M'}-2\frac{M'}{M}-\frac{t_B{}''}{t_B{}'}\right]\Bigg|_{r=0}=0\,. \tag{4.28}$$

And lastly

$$\frac{1}{(R')^2}\left(\frac{M}{2E}\right)\left[\frac{M''E'}{M'E}-6\frac{E'M'}{EM}+4\left(\frac{E'}{E}\right)^2+2\left(\frac{M'}{M}\right)^2-\frac{E''}{E}\right]\Bigg|_{r=0}=0\,.$$

However, this last expression is equivalent to equation (4.27) because if we subtract $2\times$ equation (4.25) we get $\frac{3}{2}\times$ equation (4.27).

Thus we are left with only four conditions – equation (4.25) - equation (4.28) – which relate the values of the 9 quantities M, E, t_B, M', E', t_B', M'', E'', and t_B'' at $r=0$ for a smooth central density there.

For future use, we define these quantities

$$\mathcal{A} \equiv \frac{E'M''}{EM'} - \frac{1}{2}\left(\frac{E'}{E}\right)^2 - \frac{E''}{E} \tag{4.29}$$

$$\mathcal{B} \equiv \frac{M''}{M'} - 2\frac{M'}{M} - \frac{t_B''}{t_B'}. \tag{4.30}$$

4.1.2.3 Evolution of the Second Radial Derivative of the Density

Our investigation centers on what happens to a density profile with a central maximum or minimum. To further this aim, we need to see what happens to the second radial derivative of the density. We can obtain an expression for this quantity by differentiating equation (4.5) twice with respect to R on a surface of constant time.

$$\begin{aligned}\frac{\partial_{RR}\rho}{\rho} &= \frac{2}{R}\left(\frac{3}{R} - \frac{2\,\partial_{RR}M}{\partial_R M}\right) + \frac{\partial_{RRR}M}{\partial_R M} \\ &= \frac{1}{(R')^2}\left[\frac{M'''}{M'} - 4\frac{R'M''}{RM'} - 3\frac{M''R''}{M'R'} + 6\frac{R'^2}{R^2} + 4\frac{R''}{R} + 3\frac{R''^2}{R'^2} - \frac{R'''}{R'}\right]\end{aligned} \tag{4.31}$$

where $\partial_{RRR}M$ is defined as

$$\partial_{RRR}M \equiv \left.\frac{\partial^3 M}{\partial R^3}\right|_t = \frac{1}{(R')^3}(M''' - \partial_R M R''') - \frac{3\partial_{RR}M R''}{(R')^2}.$$

A more explicit form of the above can be obtained by substituting for R', R'' and R''' into the above. We do so and at the same time repeatedly apply equations (4.25) - (4.28) ensuring a smooth central density; also using the variables defined by equations (4.1), (4.2), (4.10), (4.29) and (4.30), we find that

$$\begin{aligned}&\frac{\partial_{RR}\rho}{\rho} \times (R')^4 \\ &= \left[\frac{p^2 {t_B'}^3}{6q^3}\frac{M'}{M}\right] f_1 - \left[\frac{p^2 {t_B'}^2 v}{3q^2}\frac{M'}{M}\right] f_2 + \left[\frac{2p^2 t_B' v^2}{3q}\frac{M'}{M}\right] f_3 - \left[\frac{4p^2v^3}{3}\frac{M'}{M}\right] f_4 \\ &+ \frac{p^2}{4}\left[v^2\left(\frac{M'''}{M'} - \frac{E'''}{E'}\right) + v\frac{M'}{M}\left(\frac{M'''}{M'} - \frac{E'''}{E'}\right)\right. \\ &\left. + \frac{13\,M'\mathcal{A}v}{2\,M} - \frac{9\,M''\mathcal{A}v}{2\,M'} - \frac{M''v^3}{M'} - \frac{2\,M''v^2}{M}\right.\end{aligned}$$

$$
\begin{aligned}
&\quad -\frac{M''\,M'\,v}{M^2}-\frac{29\,M'v^3}{9\,M}+\frac{26\,M'^2v^2}{9\,M^2}+\frac{4\,M'^3v}{9\,M^3}\Bigg]\,f_5\\
&+\ \frac{2\,p^2t'_B}{q}\left[-v\left(\frac{M'''}{M'}-\frac{t'''_B}{t'_B}\right)-v\left(\frac{M'''}{M'}-\frac{E'''}{E'}\right)-\frac{M'}{M}\left(\frac{M'''}{M'}-\frac{E'''}{E'}\right)\right.\\
&\quad +\frac{9\,M''\mathcal{A}}{2\,M'}-\frac{13\,M'\,\mathcal{A}}{2\,M}+\frac{3\,M''\mathcal{B}v}{M'}-\frac{19\,M'\mathcal{B}v}{3\,M}+\frac{M''v^2}{M'}\\
&\quad \left.+\frac{8\,M''v}{M}+\frac{M''\,M'}{M^2}+\frac{76\,M'v^2}{9\,M}-\frac{94\,M'^2v}{9\,M^2}-\frac{4\,M'^3}{9\,M^3}\right]\,f_6\\
&+\ \left(\frac{pt'_B}{q}\right)^2\left[\frac{M'''}{M'}-\frac{t'''_B}{t'_B}-\frac{3\,M''\mathcal{B}}{M'}+\frac{19\,M'\mathcal{B}}{3\,M}\right.\\
&\quad \left.-\frac{6\,M''}{M}-\frac{47\,vM'}{9\,M}+\frac{68\,M'^2}{9\,M^2}\right]\,f_7\\
&+\ \frac{p^2}{4}\left[\frac{3\,M'\,\mathcal{A}v}{2\,M}+\frac{17\,M'v^3}{9\,M}+\frac{7\,M'^2v^2}{9\,M^2}\right]\,f_8\\
&+\ 2\,\frac{p^2t'_B}{q}\left[-\frac{3\,M'\,\mathcal{A}}{4\,M}-\frac{M'\,\mathcal{B}v}{2\,M}-\frac{8\,M'v^2}{9\,M}-\frac{7\,M'^2v}{9\,M^2}\right]\,f_9\\
&+\ \left(\frac{pt'_B}{3\,q}\right)^2\left[\frac{9\,M'\,\mathcal{B}}{M}-\frac{vM'}{M}+\frac{7\,M'^2}{M^2}\right]\,f_{10}\\
&+\ \frac{p^2}{4}\left[\frac{4}{3}\left(v+\frac{M'}{M}\right)\left(\frac{M'}{4\,M}-v\right)\left(\frac{M'''}{M'}-\frac{E'''}{E'}\right)\right.\\
&\quad -\frac{3\,M''\,\mathcal{A}}{2\,M}+\frac{5\,M'^2\mathcal{A}}{6\,M^2}+\frac{6\,M''\mathcal{A}v}{M'}-\frac{35\,M'\mathcal{A}v}{3\,M}\\
&\quad +\frac{4\,M''v^3}{3\,M'}+\frac{7\,M''v^2}{3\,M}+\frac{2\,M''\,M'v}{3\,M^2}-\frac{M'^2M''}{3\,M^3}\\
&\quad \left.-\frac{38\,M'v^3}{27\,M}-\frac{47\,M'^2v^2}{9\,M^2}-\frac{4\,M'^3v}{27\,M^3}+\frac{4\,M'^4}{27\,M^4}\right]\,f_{11}\\
&+\ \frac{2\,p^2t'_B}{3\,q}\left[\left(2\,v-\frac{M'}{M}\right)\left(\frac{M'''}{M'}-\frac{t'''_B}{t'_B}\right)+2\left(v+\frac{M'}{M}\right)\left(\frac{M'''}{M'}-\frac{E'''}{E'}\right)\right.\\
&\quad -\frac{9\,M''\,\mathcal{A}}{M'}+\frac{55\,M'\,\mathcal{A}}{4\,M}+\frac{3\,M''\,\mathcal{B}}{M}-\frac{11\,M'^2\mathcal{B}}{3\,M^2}\\
&\quad -\frac{6\,M''\mathcal{B}v}{M'}+\frac{79\,M'\,\mathcal{B}v}{6\,M}-\frac{2\,M''v^2}{M'}-\frac{16\,M''v}{M}\\
&\quad \left.+\frac{4\,M''\,M'}{M^2}-\frac{19\,M'v^2}{3\,M}+\frac{65\,M'^2v}{3\,M^2}-\frac{46\,M'^3}{9\,M^3}\right]\,f_{12}\\
&+\ \frac{p^2}{4}\left[\frac{2}{9}\left(v+\frac{M'}{M}\right)\left(2\,v-\frac{M'}{M}\right)\left(\frac{M'''}{M'}-\frac{E'''}{E'}\right)\right.
\end{aligned}
$$

$$+\frac{M''\mathcal{A}}{M}-\frac{5\,M'^2\mathcal{A}}{9\,M^2}-\frac{2\,M''\mathcal{A}v}{M'}+\frac{38\,M'\mathcal{A}v}{9\,M}$$
$$-\frac{4\,M''v^3}{9\,M'}-\frac{2\,M''v^2}{3\,M}+\frac{2\,M'^2M''}{9\,M^3}+\frac{76\,M'v^3}{81\,M}$$
$$+\frac{50\,M'^2v^2}{27\,M^2}-\frac{8\,M'^3v}{81\,M^3}-\frac{8\,M'^4}{81\,M^4}\Big]\,f_{13} \tag{4.32}$$

when evaluated at the origin of coordinates.

If we assume that the arbitrary functions have reasonable behaviour, such as polynomial, near the origin, then it is apparent that this expression may be simplified even more. However, time constraints forbid us from doing that here and we leave this task for another time. The expression we have obtained is, in fact, sufficient for our needs now.

We will be looking at the asymptotic values of this expression. As an indication of which terms are dominant at early and late times, the evolution functions of this quantity are plotted below. For clarity on the diagrams, we have labelled them as follows:

$$\begin{aligned}
f_1 &= \phi_6\,\phi_0+\phi_3\,\phi_1-\frac{8\,{\phi_1}^3}{\phi_0}\\
f_2 &= \phi_7\,\phi_0+\phi_4\,\phi_1+\phi_3\,\phi_2-\frac{24\,{\phi_1}^2\phi_2}{\phi_0}\\
f_3 &= \phi_8\,\phi_0+\phi_5\,\phi_1+\phi_4\,\phi_2-\frac{24\,\phi_1\,{\phi_2}^2}{\phi_0}\\
f_4 &= \phi_9\,\phi_0+\phi_5\,\phi_2-\frac{8\,{\phi_2}^3}{\phi_0}\\
f_5 &= {\phi_2}^2\\
f_6 &= \phi_1\,\phi_2\\
f_7 &= {\phi_1}^2\\
f_8 &= \phi_5\,\phi_0\\
f_9 &= \phi_4\,\phi_0\\
f_{10} &= \phi_3\,\phi_0\\
f_{11} &= \phi_2\,\phi_0
\end{aligned}$$

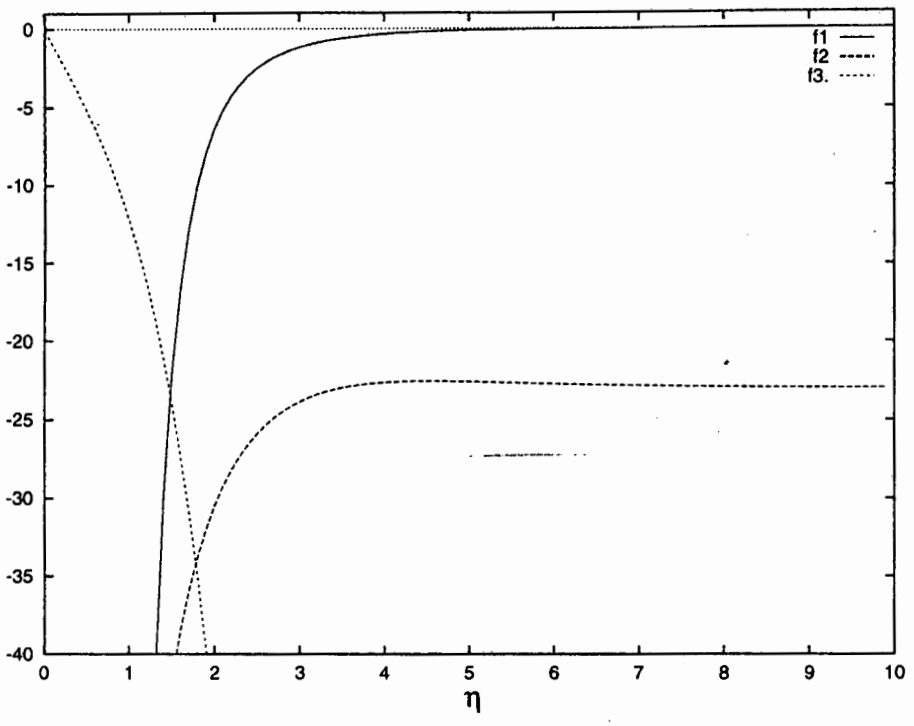

Figure 4.2: The η-functions complementary to the first three terms in $(R')^4 \times (\partial_{RR}\rho) \,/\, \rho$. The function labelled as f_2 rises to a maximum of just below -22.55 before asymptotically tending to -23.

$$f_{12} = \phi_1 \phi_0$$

$$f_{13} = {\phi_0}^2 .$$

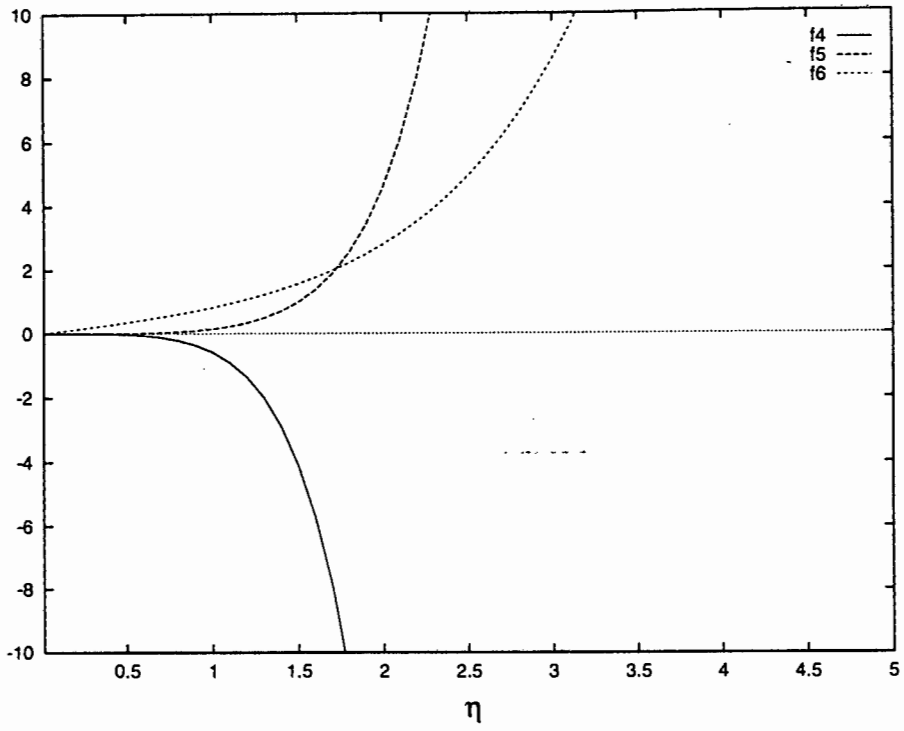

Figure 4.3: The η-functions in $(R')^4 \times (\partial_{RR}\rho) \ / \ \rho$ complementary to the fourth to sixth terms.

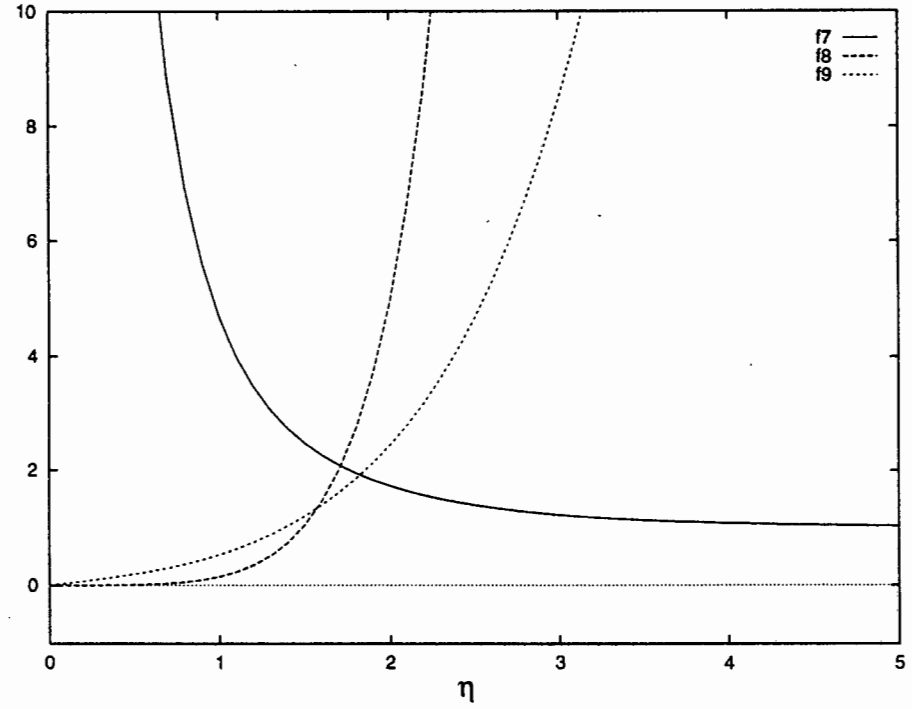

Figure 4.4: The η-functions in $(R')^4 \times (\partial_{RR}\rho) \ / \ \rho$ complementary to the seventh to ninth terms. The function f_7 asymptotically tends to 1.

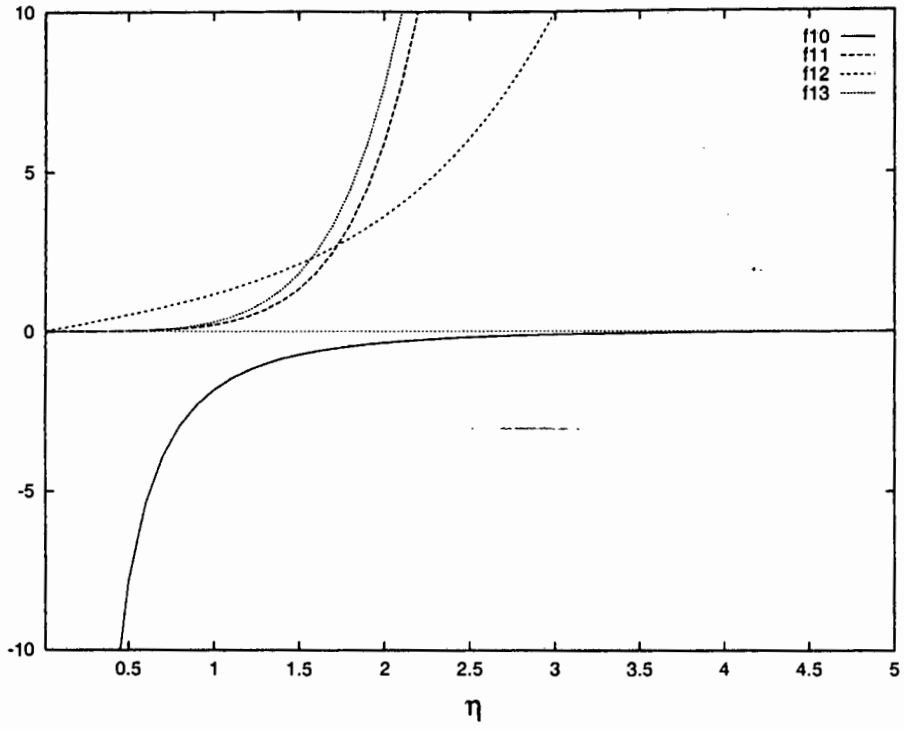

Figure 4.5: The η-functions in $(R')^4 \times (\partial_{RR}\rho) \,/\, \rho$ complementary to the tenth to thirteenth terms.

4.2 Density Profile Inversion: Existence Proof

A change in the density contrast will depend on whether factors on the right hand side of equation (4.32) change sign. We single out the dominating functions of η for early and late times. This allows us to find the relevant functions of coordinate radius r which determine this change in density profile.

We see that for small η (that is early times), $\cosh\eta \sim 1$, $\sinh\eta \sim \eta$, $\cosh\eta - 1 \sim \eta^2/2$ and $\sinh\eta - \eta \sim \eta^3/6$ which leads to a readily digestible expression when evaluated at the origin:

$$
\begin{aligned}
&\frac{\partial_{RR}\rho}{\rho}\,(R')^4 \\
&\simeq \left[\frac{(2E)^{5/2}{t'_B}^3 M'}{3M^2}\right]\left(-120\,\eta^{-5} - 22\,\eta^{-3} + \frac{181}{2520}\,\eta - \frac{23}{6048}\,\eta^3\right) \\
&+ 2Et'^2_B\left[\frac{4M'''}{M'} - \frac{4t'''_B}{t'_B} + \frac{70M''}{3M} - \frac{18M'^2}{M^2}\right. \\
&\quad \left. - \frac{70M't''_B}{3Mt'_B} - \frac{12M''^2}{M'^2} + \frac{12M''t''_B}{M't'_B}\right]\eta^{-2} \\
&+ 2Et'^2_B\left[\frac{7M'E'}{6ME} - \frac{79M'^2}{18M^2} + \frac{2M'''}{3M'} - \frac{2t'''_B}{3t'_B}\right. \\
&\quad \left. + \frac{79M''}{18M} - \frac{79M't''_B}{18Mt'_B} - \frac{2M''^2}{M'^2} + \frac{2M''t''_B}{M't'_B}\right] \\
&+ \frac{Mt'_B}{\sqrt{2E}}\left[-\frac{M'''}{3M} + \frac{M't'''_B}{3Mt'_B}\right. \\
&\quad \left. - \frac{11M''M'}{9M^2} + \frac{4M'^3}{9M^3} + \frac{M''^2}{M'M} - \frac{M''t''_B}{Mt'_B} + \frac{11M'^2t''_B}{9M^2t'_B}\right]\eta \\
&+ 2Et'^2_B\left[\frac{13M'E'}{70ME} - \frac{167M'^2}{840M^2} + \frac{M'''}{60M'} - \frac{t'''_B}{60t'_B}\right. \\
&\quad \left. + \frac{7M''}{72M} - \frac{7M't''_B}{72Mt'_B} - \frac{M''^2}{20M'^2} + \frac{M''t''_B}{20M't'_B}\right]\eta^2 \\
&+ \frac{Mt'_B}{\sqrt{2E}}\left[\frac{2M''M'}{27M^2} - \frac{31M'^3}{270M^3} - \frac{M'''}{45M}\right. \\
&\quad \left. + \frac{11M'^2E'}{30M^2E} - \frac{M'''E'}{10M'E} + \frac{E't'''_B}{20Et'_B} + \frac{M't'''_B}{45Mt'_B}\right.
\end{aligned}
$$

$$
\begin{aligned}
&+\frac{E'''}{20\,E}+\frac{M''^2}{15\,M'\,M}-\frac{M''\,t_B''}{15\,M t_B'}-\frac{2\,M'^2 t_B''}{27\,M^2 t_B'}\\
&-\frac{11\,E'\,M''}{15\,EM}+\frac{3\,M''^2 E'}{10\,M'^2 E}-\frac{3\,M''\,E''}{20\,M'\,E}+\frac{19\,M'\,E''}{60\,ME}\\
&-\frac{3\,M''\,E'\,t_B''}{20\,M'\,E t_B'}+\frac{5\,M'\,E'\,t_B''}{12\,ME t_B'}\Bigg]\,\eta^3\\
+\;&2Et_B'^2\Bigg[-\frac{M'\,E'}{168\,ME}+\frac{M'^2}{144\,M^2}-\frac{M'''}{1512\,M'}+\frac{t_B'''}{1512\,t_B'}\\
&-\frac{5\,M''}{1296\,M}+\frac{5\,M'\,t_B''}{1296\,M t_B'}+\frac{M''^2}{504\,M'^2}-\frac{M''\,t_B''}{504\,M'\,t_B'}\Bigg]\,\eta^4
\end{aligned}
\tag{4.33}
$$

with R' at early times given by

$$
R'|_{\eta\to 0}\simeq\frac{1}{12}\frac{M'}{E}\eta-4Et_B'\eta^{-1}\,.
$$

We have used equation (4.26) again and neglected terms of order η^5 and higher. (Although our main consideration should only be the relative strengths of the different modes, we deem it appropriate to proceed as above because any term of order η^5 or higher will inevitably tend to zero as $\eta\to 0$ once we include the factor of η^4 that arises from R'^4 at early times on the left hand side of the above equation.)

We consider the late time behaviour of the functions of parameter time η in equation (4.32). We note that $\sinh\eta\to\cosh\eta$, $\cosh\eta-1\to\cosh\eta$ where $\cosh\eta\to e^\eta/2$ as $\eta\to\infty$. Therefore for large η, and at the origin,

$$
\begin{aligned}
&\frac{\partial_{RR}\rho}{\rho}\,(R')^4\\
&\simeq\;\left(\frac{M}{2E}\right)^2\Bigg[-\frac{3\,M''^2E'^2}{4\,M'^2E^2}+\frac{3\,M''\,E'\,E''}{4\,M'\,E^2}-\frac{5\,M'\,M''\,E'}{18\,M^2E}-\frac{5\,M'\,E'\,E''}{6\,ME^2}\\
&\quad+\frac{5\,M'^2E''}{18\,M^2E}+\frac{5\,M''\,E'^2}{6\,ME^2}+\frac{M'''E'^2}{4\,M'\,E^2}-\frac{E'\,E'''}{4\,E^2}\\
&\quad+\frac{5\,M'^2E'^2}{36\,M^2E^2}-\frac{5\,M'E'^3}{12\,ME^3}+\frac{E'^4}{4\,E^4}\Bigg]\cosh^2\eta\\
+\;&\Bigg\{\frac{Mt_B'}{\sqrt{2E}}\Bigg[\frac{11\,M''\,M'}{9\,M^2}-\frac{58\,M'^3}{27\,M^3}-\frac{13\,M'E'^2}{6\,ME^2}+\frac{6\,M'^2E'}{M^2E}
\end{aligned}
$$

$$
\begin{aligned}
&-\frac{M'''E'}{M'E}+\frac{E't_B'''}{2Et_B'}+\frac{E'''}{2E}-\frac{11M'^2t_B''}{9M^2t_B'}\\
&-\frac{19E'M''}{3EM}+\frac{3M''^2E'}{M'^2E}-\frac{3M''E''}{2M'E}+\frac{8M'E''}{3ME}\\
&-\frac{3M''E't_B''}{2M'Et_B'}+\frac{11M'E't_B''}{3MEt_B'}\Bigg]\\
&+\left(\frac{M}{2E}\right)^2\left[-\frac{3M'E'^3}{ME^3}+\frac{23M'^2E'^2}{4M^2E^2}-\frac{19M'^3E'}{6M^3E}-\frac{9M''E'^2}{4ME^2}\right.\\
&\left.+\frac{9M'E'E''}{4ME^2}+\frac{4M'^4}{9M^4}+\frac{3M'M''E'}{2M^2E}-\frac{3M'^2E''}{2M^2E}\right]\Bigg\}\cosh\eta\\
+&\left\{2Et_B'^2\left[\frac{11M'E'}{3ME}-\frac{68M'^2}{9M^2}+\frac{M'''}{M'}-\frac{t_B'''}{t_B'}\right.\right.\\
&\left.+\frac{19M''}{3M}-\frac{19M't_B''}{3Mt_B'}-\frac{3M''^2}{M'^2}+\frac{3M''t_B''}{M't_B'}\right]\\
&+\frac{Mt_B'}{\sqrt{2E}}\left[\frac{M'E'^2}{ME^2}-\frac{3M'^2E'}{M^2E}+\frac{11M'^3}{9M^3}+\frac{3E'M''}{EM}\right.\\
&\left.\left.-\frac{3M'E't_B''}{2MEt_B'}-\frac{M''M'}{M^2}+\frac{M'^2t_B''}{M^2t_B'}-\frac{3M'E''}{2ME}\right]\right\}\\
+&\ 2Et_B'^2\left[-\frac{M''}{M}+\frac{10M'^2}{9M^2}+\frac{M't_B''}{Mt_B'}+\frac{M'E'}{6ME}\right]\cosh^{-1}\eta\\
+&\left[\frac{(2E)^{5/2}t_B'^3M'}{3M^2}\right]\left(\cosh^{-2}\eta-8\cosh\eta^{-1}\right)
\end{aligned}
\tag{4.34}
$$

where R' at late times is given by

$$
R'|_{\eta\to\infty}\simeq\frac{1}{4}\frac{ME'}{E^2}\cosh\eta-\sqrt{2E}t_B'\,.
$$

We have used condition (4.26) here as well.

A comparison of these two expressions will determine the conditions under which a density profile changes from a maximum to a minimum.

We recall that there are four restrictions on E, E', E'', M, M', M'', t_B, t_B' and t_B'' given by equations (4.25) - (4.28). This leaves us with some freedom to fix the above expressions at $r=0$. In addition there are also the conditions for a regular origin (section 2.2.2) and those for no shell crossings (Table 2.1). However, the former conditions do not provide any new

constraints and the latter are inequality constraints which are not as severe as the others.

We can choose the arbitrary functions in such a way as to let any particular evolutionary mode disappear. For instance, we could choose the functions in such a way that for early times the η term is dominant and for late times, the $\cosh^2\eta$ term is the leading one. Then we can see that in the resulting expression for equation (4.33) there occurs a term of t_B''' which does not occur in the resulting expression for equation (4.34). This allows us to fix the early time behaviour of the density. And, likewise, there occurs a term of E''' at late times which does not occur at early times for the relative change in concavity of the density. Thus, in principle, we should be able to fix the late time behaviour as well due to this freedom. We also note that the term M''' is free and this allows us to investigate possible 'middle time' behaviour as well.

4.3 Specific Models

We will consider an initial overdensity changing to an underdensity. So, at early times at the origin, we want the change in concavity to be negative and at late times, positive. We are also preventing shell-crossing singularities from interfering and for this we use the conditions for no shell-crossings as in Table 2.1. These are, for $R' > 0$ and $E > 0$,

$$t_B' \leq 0\,, \quad E' > 0 \quad \text{and} \quad M' \geq 0\,.$$

It is not easy specifying the arbitrary functions in a way which would satisfy the various restrictions we require and be conducive to a systematic analysis. We thus consider 'perturbations'[4] of an FLRW model in the following way:

$$M(r) = M_0 r^3(1+\alpha(r)), \quad \alpha(0)=0\,; \tag{4.35}$$

$$2\,E(r) = r^2(1+\beta(r)), \quad \beta(0)=0\,; \tag{4.36}$$

[4]Once again, this is just a mathematical device as was the case previously for the 'underlying model' of section 3.2.2.1. No averaging or matching procedure to define a background FLRW model has been employed.

$$t_B(r) \;=\; \gamma(r), \quad \gamma(0) = 0\,. \tag{4.37}$$

These ensure the origin conditions of section 2.2.2 are satisfied. However, they do not necessarily satisfy the restrictions imposed by (4.25) - (4.28).

These functions are just a sum of an FLRW term with a perturbation and thus we expect all variation in density to come just from the perturbation functions $\alpha(r)$, $\beta(r)$ and $\gamma(r)$.

For perturbation functions of the form

$$\alpha(r) \;=\; Ar^a\,, \tag{4.38}$$

$$\beta(r) \;=\; Br^b\,, \tag{4.39}$$

$$t_B(r) \;=\; Cr^c\,, \tag{4.40}$$

the requirement of no shell-crossings leads to the following restrictions on the constants A, B and C:

$$t_B' \leq 0 \;\Rightarrow\; C \leq 0 \tag{4.41}$$

$$M' \geq 0 \;\Rightarrow\; A \geq -\frac{3}{(3+a)\,r^a} \tag{4.42}$$

$$E' > 0 \;\Rightarrow\; B > -\frac{2}{(2+b)\,r^b} \tag{4.43}$$

The smooth central density criteria – that is, in this case, (4.26) and (4.28) for $t_B(r)$ (Table 4.1) or (4.27) for $M(r)$ and $E(r)$ – impose the following restrictions on A, B and C (Tables 4.2 and 4.1). For simplicity, we will only investigate models where a, b and c are natural numbers.

$c = 1$	$C = 0$
$c \geq 2$	no restrictions

Table 4.1: Restrictions imposed on the perturbation t_B by the requirement of a flat central density ($\forall c \in \mathbb{N}^+$) .

	$a=1$	$a \geq 2$
$b=1$	$A=B$	$B=0$
$b \geq 2$	$A=0$	no restrictions

Table 4.2: Restrictions imposed on the perturbations to E and M by the requirement of a flat central density $(\forall a, b \in \mathbb{N}^+)$.

We use equation (4.33) to determine the early time behaviour and choosing the bangtime function to be smooth and vanishing at the origin ($\gamma'(0) = 0$), we find that the leading nonzero component of $\left.\frac{\rho_{RR}}{\rho}\right|_{r=0}$ is the η mode, and in R' the term that survives is the first one, which results in the following expression which we will use to obtain results in this section.

$$\lim_{\eta\to 0} \left.\frac{\partial_{RR}\rho}{\rho}\right|_{r=0} \simeq \left(\frac{12E}{M'}\frac{1}{\eta}\right)^3 6\sqrt{2E}t'_B \left[\frac{4}{9}\frac{M'^2}{M^2} + \frac{1}{3}\left(\frac{t'''_B}{t'_B} - \frac{M'''}{M'}\right) + \left(\frac{M''}{M'} - \frac{t''_B}{t'_B}\right)\left(\frac{M''}{M'} - \frac{11}{9}\frac{M'}{M}\right)\right] . \tag{4.44}$$

Using a bangtime function $t_B = Cr^2$, substitution into equation (4.44) shows that the relative concavity of the density at early times can be fixed as negative by choosing t_B as a decreasing function[5]: in fact,

$$\lim_{\eta\to 0} \left.\frac{\partial_{RR}\rho}{\rho}\right|_{r=0} = \frac{160C}{{M_0}^3} .$$

A choice of t_B which is of higher power gives $\frac{\partial_{RR}\rho}{\rho} = 0$ at the origin at early times.

We use equation (4.34) to determine the late time behaviour and we select only the dominating function of η which gives us the first term in this equation. In R' the term that survives is again the first one resulting in the following expression after using conditions (4.25) and (4.27).

$$\lim_{\eta\to\infty} \left.\frac{\partial_{RR}\rho}{\rho}\right|_{r=0} \simeq \left(\frac{4E^2}{ME'}\frac{1}{\cosh\eta}\right)^2 \left[-\frac{1}{4}\frac{E'^2}{E^2} + \frac{M'''}{M'} - \frac{E'''}{E'} + \left(\frac{E''}{E'} - \frac{M''}{M'}\right)\left(3\frac{M''}{M'} - \frac{5}{2}\frac{E'}{E}\right)\right] . \tag{4.45}$$

[5]This automatically satisfies the first requirement for no shell crossings to occur as well.

We should be able to fix this by suitable choices of α and β: the results after use of Table 4.2 are tabulated below (Table 4.3).

	$a=1$	$a=2$	$a\geq 3$
$b=1$	$1/2\,(-A/r+A^2)$	$2A$	0
$b=2$	$-3B$	$2A-3B$	$-3B$
$b\geq 3$	0	$2A$	0

Table 4.3: The late time value of $(\partial_{RR}\rho)\,/\,\rho$ at the origin multiplied by M_0.

Clearly there are a wide variety of models which can change concavity at the origin and which also have no shell crossing singularities. We will illustrate DPI on a model which has quadratic perturbation functions – that is; a, b and c are all equal to two. We choose $A = 100$, $B = 1 \times 10^{-6}$ and $C = -3 \times 10^{-8}$. Since we are only interested in qualitative results, we may put $M_0 = 1$[6]. The density profile this determines is plotted for various values of cosmic time t obtained by a bisection method employing the second half of equation (4.3).

The units are converted as follows

$$\begin{aligned} 1\ ctu &= 2.005 \times 10^{9} yrs \\ 1\ clu &= 6.146 \times 10^{8} pc \\ 1\ cmu &= 1.285 \times 10^{22} M_{\odot} \\ 1\ cmu\,/\,clu^3 &= 3.746 \times 10^{-27} yrs \end{aligned} \tag{4.46}$$

[6]With an FLRW origin this would be $M_0 = \dfrac{2q_0}{H_0(1-2q_0)^{3/2}}$.

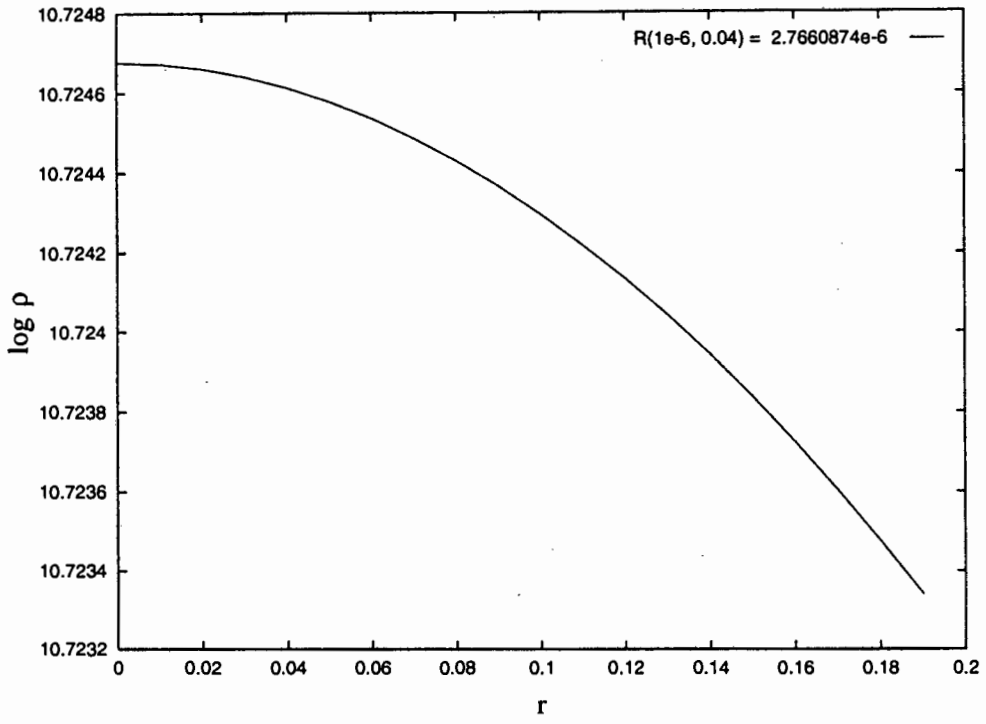

Figure 4.6: The density profile on a worldline at an early time ($t = 1 \times 10^{-6} \sim 2000yrs$). In these figures, the core is taken to be the value of R at the comoving radius $r = 0.04$ and they all use base 10 logs. At this time the value corresponds to an overdensity of about 1.7 kpc in diameter which corresponds to the size of a small galaxy today. The units in all the figures are cosmological. The value of the density at the origin $\rho_0 \sim 2.0 \times 10^{-16} g/cc$.

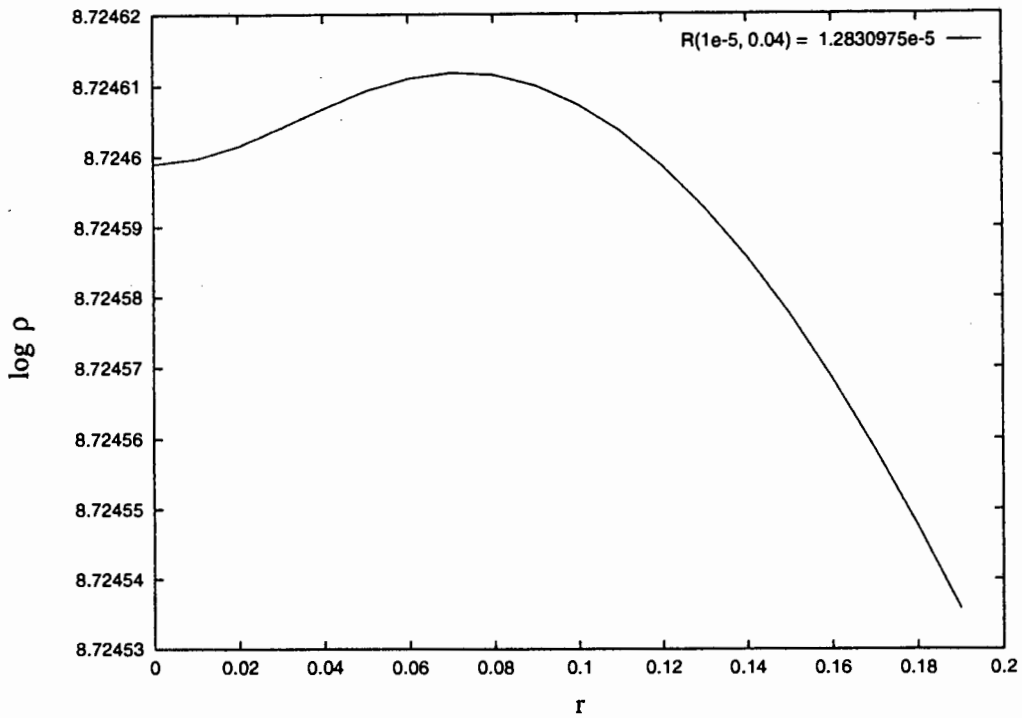

Figure 4.7: The density profile on a worldline at a later time. This diagram and the next one illustrate the change in concavity at the centre, which occurs when the universe was $\sim 2 \times 10^4$ years old. $R \sim 7.9kpc$ and $\rho_0 \sim 2.0 \times 10^{-18} g/cc$.

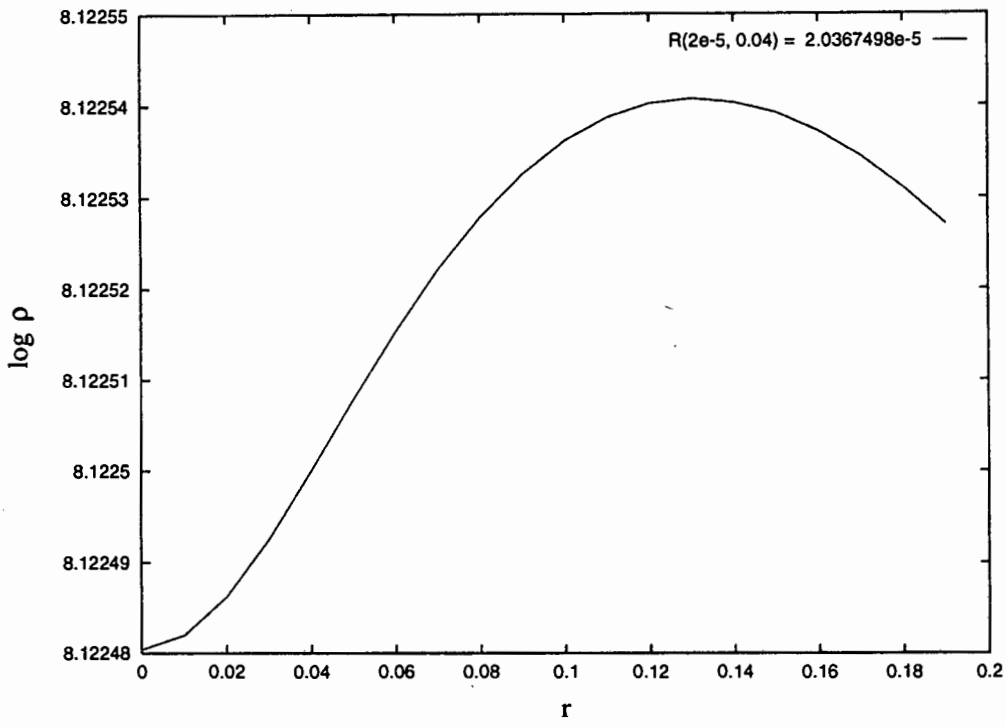

Figure 4.8: The density profile on a worldline at a still later time which, when compared to the previous figure, illustrates the movement of the maximum away from the centre. This is as we expected and shows that a density wave must exist near the origin if the profile inverts on the central worldline. $t \sim 4 \times 10^4 yrs$, $R \sim 12.5 kpc$ and $\rho_0 \sim 5 \times 10^{-19} g/cc$.

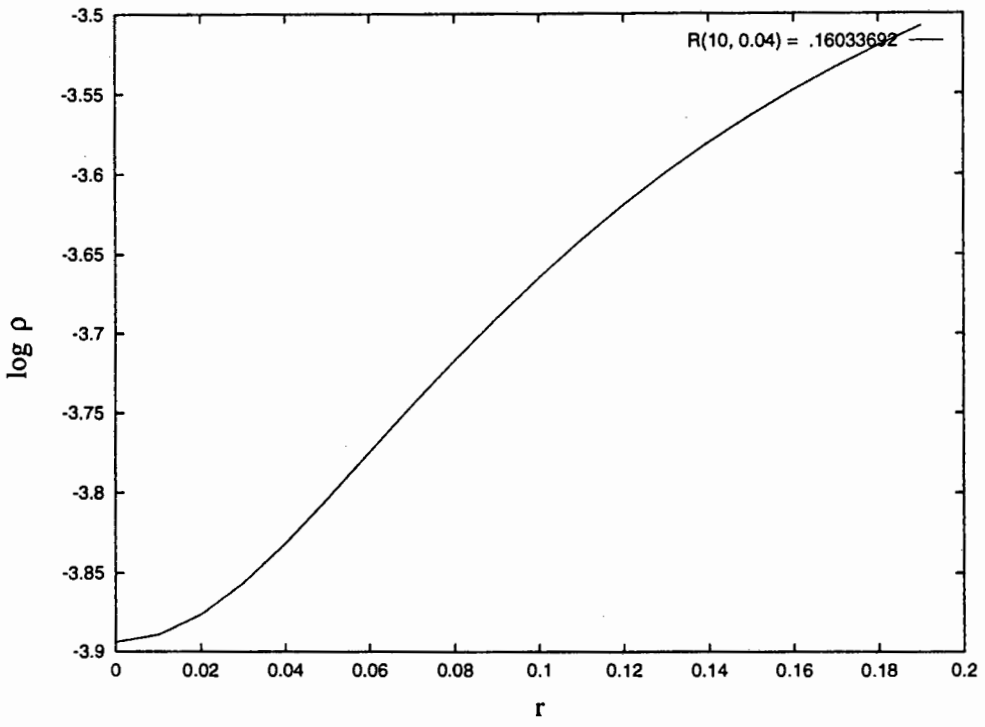

Figure 4.9: The density profile on the worldline today ($t \sim 20Gyrs$). This corresponds to a void (albeit one with a rather elongated wall) with a diameter of approximately $100Mpc$. $\rho_0 \sim 5 \times 10^{-31} g/cc$ and the maximum density on this diagram is $\rho_m \sim 10^{-3.5} \sim 1.2 \times 10^{-30} g/cc$.

4.4 Implications and Discussion

Perhaps the most important implications of this work derive from the existence proof of the possibility of DPI and density waves in the (very symmetrical) LTB model[7]. In the real universe, which is much more complex than this model, we expect waves to be generic [21]. The crucial element in our investigation is the importance of the bangtime function t_B and its derivatives at early times. We may recall from section 2.2 that t'_B generates the decaying mode and E' the growing mode to RW perturbations. The overdensity occurs at early times because we choose t_B in such a way that it results in an overdensity and, in a similar fashion, the underdensity occurs at a late time because we choose E such that it gives that particular type of density profile. Perhaps the reason why the effect obtained here has not been discussed before is because most studies consider linearised perturbations which have the ultimate effect of neglecting the decaying mode.

The most intricate model of structure formation assumes Cold Dark Matter (CDM) with a Harrison-Zel'dovich spectrum of initial perturbations. Observations indicate that CDM predictions on large scales and small scales are incompatible. In particular, standard CDM has trouble reproducing the large velocity dispersion of luminous matter from the stationary standpoint. The bulk streaming flows observed are probably larger than can be produced by standard CDM. Realising the fairly universal failings of standard structure formation theories to explain bulk flow statistics, one might argue that there is some fundamental assumption that must be re-evaluated unless there is a radically different process responsible for structure in the universe. It seems natural to ask if our results might go at least some way in solving these problems.

In the linear theory of structure formation, the topology of density contour surfaces does not change. No links are formed and no chains are broken – the genus of the surface is

[7] as has been numerically discovered previously in many studies (in LTB and related models) on large scale structures, mentioned in the introduction to this chapter.

unchanged since the process is continuous. When nonlinearity is important, the genus of the surfaces evolves as clumps and bubbles form. Even though the statistics today may be non-Gaussian, their structure today will vary depending on the Gaussianity of the initial distribution. However, the way that this occurs will be different if the density profile inverts and if density waves are present, since no longer will overdense regions simply grow monotonically. There will be a sophisticated interchange of spatial and temporal densities. This means that density waves must be included if a correct interpretation of topological studies of structure formation is to be obtained. Thus the change to the topology of the constant density contours, comparing density waves and no-density waves scenarios, should be examined.

A direct effect of DPI is its implications for the transfer function used ubiquitously in standard structure formation theories whereby luminous matter congregates in the peaks of the underlying mass distribution . These peaks do not move; in the sense that they remain attached to the same world line as time evolves. The only change that happens is the infall of matter about these peaks so that the density contrast increases. There is spatial flow of matter, but the spatial distribution of extrema of the initial density field remains invariant. This invariance is broken when DPI occurs. The effect is to (amongst other things) change the form of the transfer function. We could reasonably speculate that the transfer function becoming more complicated may perhaps allow one to take a standard scale invariant spectrum and fit it to small, large and intermediate constraints.

Chapter 5

Conclusion

My pen is at the bottom of a page,
Which, being finished, here the story ends;
'Tis to be wished it had been sooner done,
But stories somehow lengthen when begun.

– George Gordon, Lord Byron

We have shown how the LTB model is used to model some aspects of our universe. Looking mainly at the matter content and density structures the inhomogeneity allows us to model, we have also discussed other areas of application and mentioned the fundamental question of Cosmic Censorship which is unresolved to this day mainly due to the counterexamples found in the LTB model.

In both of the in-depth studies conducted in this contribution, we have found positive results to the questions raised. That is, we have shown that the effects of purely radial inhomogeneity distorts the redshift-area distance relation obtained from modelling the universe as a smooth homogeneous universe – even in the case of a flat universe. This was accomplished by writing the usual solutions for LTB models in terms of quantities on the null cone, averaging the density on a constant time slice to obtain a background FL model and then comparing null cone quantities in the 'real' and background models. We have also

shown that purely gravitational evolution may cause peaks in density to change to troughs (and conceivably vice versa) on cosmological (or near-cosmological) scales. This was done by finding the curvature of the density profile at the origin and showing that it can in general be positive or negative for any time we may choose.

As has been pointed out in the conclusion to each of these studies, there is much scope for further work on these, or related, topics. In particular, the results of chapter 3 which illustrate the concept of radial lensing, when viewed in conjunction with the formation of caustics and thus the phenomenon of shrinking has important and far-reaching consequences for the validity of lensing effects on *large angular-scale* number counts and CMB investigations. In addition, the technique of using the null cone gauge, whilst retaining the comoving character of the usual variables, in LTB models first employed there opens up the way for analytical studies of observations in these models. Chapter 4 which has as its central element the existence proof for density waves in LTB models has implications for standard structure formation and evolution theory which, we suggest, suffers perhaps from its stationary character.

I believe these investigations go some way in supporting the contention that the LTB universe has definite interest as a type of 'test universe' to illustrate the subtleties of Einsteins theory of General Relativity. Furthermore, until the Copernican Hypothesis can be shown to be more than just a working hypothesis, it must be considered a very good model (on equal footing perhaps with the FLRW universes) of the post-decoupling universe. But these considerations must be weighed against experiment and other theoretical results. Most notably, the measured near-isotropy of the CMB when combined with the almost-EGS[1] result recently proven by Stoeger et al [65] and a Copernican assumption indicate that a theory of linearised perturbations around an RW background is probably applicable on the largest scales. Thus the one useful feature of the LTB models – their overt nonlinearity – may not

[1]EGS refers to the Ehlers-Gehren-Sachs theorem which states that an isotropic CMB combined with CH means that the universe is FLRW.

always be needed to describe situations of this nature. However, we do know that at later times, the dynamics become non-linear and perhaps here the model comes into its own when we are dealing with what may be considered processes of an astrophysical nature or at the interface of astrophysics and cosmology.

On the other hand, whilst it is geometrically richer than the FLRW models, there is naturally a price one has to pay for this. One shortcoming is the fact that one has to assume a pressureless fluid to be able to obtain a complete solution to the EFE. The other, more practical problem is that it is difficult to find *tractable* problems which suit themselves to a spherically symmetric inhomogeneous universe. Indeed, the problem of how to handle quantities on the null cone have until recently not been solved analytically. Finally, it must be realised that although the model is inhomogeneous, it still does not come close to the real universe out there which is clearly not spherically symmetric. The vast theory of perturbations in cosmology probably offers the best route forward in this field. Even here though, one feels that the LTB model may be useful in investigating the regions of applicability, in the radial direction, of these (usually) linearised perturbations. The other side of the coin is, of course, that the very symmetry which allows us to solve the field equations exactly to obtain this solution may obscure what is truly generic in the real universe. Thus there is perhaps a need to perturb the LTB model around some open solution domain to find out how stable this exact solution is. This is, of course, a general problem in Relativity and Cosmology.

We can fairly say that the cosmology we have used in this work is a reasonable mathematical model for illustrating how complex our universe really is – even in relatively simple situations – and how careful one must be when one does physics in a simplified model of it.

Bibliography

[1] Adams, F.C. and Fatuzzo, M. 1993, *Astrophys. J.*, **403**, 142.

[2] Arnau, J.V., Fullana, M.J., Monreal, L. and Saez, D. 1993, *Astrophys. J.*, **402**, 359.

[3] Barnes, A. and Whitrow, G.J. 1970, *Mon. Not. Roy. Astron. Soc.*, **148**, 193.

[4] Bondi, H. 1947, *Mon. Not. Roy. Astron. Soc.*, **107**, 410.

[5] Bonnor, W.B. 1974, *Mon. Not. Roy. Astron. Soc.*, **167**, 55.

[6] Bonnor, W.B. 1985, *Class. Quantum Grav.*, **2**, 781.

[7] Bonnor, W.B. and Chamorro, A. 1991, *Astrophys. J.*, **378**, 461.

[8] Burnett, G. 1993, *Phys. Rev. D48*, **12**, 5688 .

[9] Christodoulou, D. 1984, *Comm. Math. Phys.*, **93**, 171.

[10] Clarke, C.J.S. 1993, 'The Cosmic Censorship Hypothesis', in *The Renaissance of General Relativity and Cosmology* eds. Ellis, G.F.R., Lanza, A. and Miller, J.C.

[11] Coles, P. and Ellis, G.F.R. 1994, *Nature*, **370**, 609.

[12] Darmois, G. 1927, *Mémorial des Sciences Mathematiques*, Fasc.**25**, Gaulthier-Villars, Paris.

[13] Datt, B. 1938, *Zeitshrift fur Physik*, **108**, 314.

[14] Dekel, A. 1994, *Ann. Rev. Astron. & Astrophys.*, **32**.

[15] Dyer, C.C. and Roeder, R.C. 1972, *Astrophys. J.*, **174**, L115.

[16] Eardley, D.M. 1987, in: *Gravitation and Astrophysics.* ed. B. Carter and J. Hartle (New York and London: Plenum).

[17] Eardley, D.M. and Smarr, L. 1979, *Phys. Rev. D*, **19**, 2239.

[18] Ellis, G. F. R. 1967, *J. Math. Phys.*, **8**, 1171.

[19] Ellis, G. F. R. 1980, *Ann. New York Acad. Sci.*, **336**, 130-160.

[20] Ellis, G.F.R, Bassett, B.A.C.C and Dunsby, P.K.S. 1996, *UCT preprint.*

[21] Ellis, G.F.R., Hellaby, C.W. and Matravers, D.R. 1990, *Astrophys. J.*, **364**, 400.

[22] Ellis, G.F.R. and Schmidt, B.G. 1977, *Gen. Rel. Grav.* **8**, 915.

[23] Ellis, G.F.R. and Stoeger, W. 1988, *Class. Quant. Grav.*, **5**, 207.

[24] van Elst, H. *private communication.*

[25] van Elst, H. and Ellis, G.F.R. 1996, *Class Q. Grav.*,**13**, 1099-1127.

[26] Griffiths, J.B. 1991, *Colliding Plane Waves in General relativity* (Oxford Science Publications).

[27] Hawking, S. W. and Penrose, R. 1970, *Proc. Roy. Soc. Lond.*, **A314**, 529 - 548.

[28] Hellaby, C.W. 1985, *PhD thesis*, Queens University, Kingston, Ontario.

[29] Hellaby, C.W. 1987, *Class. Q. Grav.*, **4**, 635-650.

[30] Hellaby, C.W. 1994, *Phys. Rev. D*, **49**, 6484-8.

[31] Hellaby, C.W. and Lake, K. 1984, *Astrophys. J.*, **282**, 1-10 and errata in 1985 *ibid* **294**, 702.

[32] Hellaby, C. and Lake, K. 1985, *Astrophys. J.*, **290**, 381-9 and errata in 1986 *ibid* **300**, 461.

[33] Henriksen, R.N. and de Robertis, M. 1980, *Astrophys. J.*, **240**, 917.

[34] Humphreys, N.P., Maartens, R. and Matravers, D.R. 1996, *Portsmouth University preprint* RCG 96/1.

[35] Israel, W. 1966, *Il Nuovo Cim.*, **44B**, 1 and errata in *ibid* 1967 **48B**, 463.

[36] Krasiński, A. 1993 *UCT preprint 10.*

[37] Krasiński, A. and Perkowski, M. 1981, *Gen. Rel. Grav.*, **13**, 67.

[38] Kriele, M. 1997 *Class. Q. Grav.*, **14**, 153.

[39] Lake, K. 1984, *Phys. Rev. D*, **29**, 771.

[40] Lake, K. and Pim, R. 1985, *Astrophys. J.*, **298**, 439.

[41] Landau, L.D. and Lifshitz, E.M. 1975, *The Classical Theory of Fields* (Pergamon).

[42] de Lapparent, V., Geller, M.J. and Huchra, J.P. 1986, *Astrophys. J.*, **302**, L1.

[43] Lemaître, G. 1931, *Mon. Not. Roy. Acad. Sci.*, **91**, 483.

[44] Lemaître, G. 1933, *Ann. Soc. Scient. Bruxelles*, **A53**, 51.

[45] Linde, E.V. 1988, *Astron. and Astroph.*, **206**, 190.

[46] MacCallum, M. 1993, 'Anisotropic and Inhomogeneous Relativistic Cosmologies', in *The Renaissance of General Relativity and Cosmology* eds. Ellis, G.F.R., Lanza, A. and Miller, J.C.

[47] Maartens, R., Humphreys, N.P., Matravers, D.R. and Stoeger, W. 1996, *Class. Q. Grav.*, **13**, 253-264. (gr-qc/9511045).

[48] Maeda, K., Sasaki, M. and Sato, H. 1983, *Progr. Theor. Phys.*, **69**, 89.

[49] Mattaresse, S., Pantano, O. and Saez, D. 1993, *Phys. Rev. D*, **47**, 1311.

[50] Mészarós, A. 1991, *Mon. Not. Roy. Astron. Soc.*, **253**, 619.

[51] Occhionero, F., Vignato, A. and Vittorio, N. 1978, *Astron. and Astroph.*, **70**, 265.

[52] Olson, D.W. and Silk, J. 1979, *Astrophys. J.*, **233**, 395.

[53] Omer, G.C. 1965, *Proc. Nat. Acad. Sci.* USA, **53**, 1.

[54] Padmanabhan, T. 1993, *Structure Formation in the Universe* (Cambridge: Cambridge University Press).

[55] Papapetrou, A. 1978, *Ann. Inst. H. Poincaré*, **29**, 207.

[56] Pim, R. and Lake, K. 1986, *Astrophys. J.*, **304**, 75.

[57] Raine, D.J. and Thomas, E.G. 1981, *Mon. Not. Roy. Astron. Soc*, **195**, 649.

[58] Rubin, V.C. and Coyne, G. V., S.J. 1988, *Large-Scale Motions in the Universe* (Princeton: Princeton University Press).

[59] Sato, H. 1982, *Progr. Theor. Phys.*, **68**, 236.

[60] Sato, H. 1984, in: *General Relativity and Gravitation.* ed. B. Bertotti, F. de Felice and A. Pascolini (Dordrecht: Reidel), 289.

[61] Schneider, P., Ehlers, J. and Falco, E.E. 1992, *Gravitational Lenses* (Berlin: Springer Verlag).

[62] Seljak, U. 1994, *Astrophys. J.*, **425**, L1.

[63] Silk, J. 1977, *Astron. and Astroph.*, **59**, 53.

[64] Solomons, D. and Ellis, G.F.R. *in preparation.*

[65] Stoeger, W., Maartens, R. and Ellis, G.F.R. 1995, *Astrophys. J.*, **443**, 1.

[66] Szekeres, P. 1975, *Phys. Rev. D12*, **10**, 2941.

[67] Tavakol, R.K. and Ellis, G.F.R. 1988, *Phys. Lett. A*, **130**, 217.

[68] Tolman, R.C. 1934, *Proc. Nat. Acad. Sci.*, **20**, 169.

[69] Tolman, R.C. 1934, *Relativity, Thermodynamics and Cosmology* (Oxford: Clarendon Press).

[70] Walsh, D., Carswell, R.F. and Weymann, R.J. 1979, *Nature*, **279**, 381.

[71] Weinberg, S. 1972, *Gravitation and Cosmology* (New York: Freeman).

[72] Weinberg, S. 1976, *Astrophys. J.*, **208**, L1-3.

[73] Yodzis, P., Mueller zum Hagen, H. and Seifert, H. 1973-4, *Comm. Math. Phys.*, **34** 135 and *ibid* **37**, 29.

[74] Zel'dovich, Ya. B. and Grischuk, L.P. 1984, *Mon. Not. Roy. Astron. Soc*, **207**, 23P.

Acknowledgements

I would like to thank my supervisors, Charles Hellaby and George Ellis, for their patient supervision of my efforts. I would not have been able to complete this work were it not for them and others like them who have helped me through the difficult stages and also the easy ones! The likes of Bruce ('evil Bruce') Bassett, Tim Gebbie and the other guys in the Cape Town Cosmology group (Deon, Rodney, Conrad, Kamilla, Nico, Michael and others past and present?) all spring to mind. Without the many interesting times and discussions we have shared I doubt that I would know very much about life and this game in particular. Ooh! and let me not forget the lab crew (the midnight detail). Thanks to Kevin in particular for helping with those computer queries. Of equal importance are the people who have been a support base to me throughout this period of intensive (and sometimes not so intensive) study; my thanks to my family and close friends.

Nazeem Mustapha

Desunt nonnulla